Title: Stable source of Holocene spring precipitation recorded in leaf wax hydrogen-isotope ratios from two New York lakes.

Authors: Anna K. Schartman[a]*, Aaron F. Diefendorf[a], Thomas V. Lowell[a], Erika J. Freimuth[a], Alexander K. Stewart[b], Joshua D. Landis[c], Benjamin R. Bates[a]

[a] Department of Geology, University of Cincinnati, Cincinnati, OH 45221, USA

[b] Department of Geology, St. Lawrence University, Canton, NY 13617, USA

[c] Department of Earth Sciences, Dartmouth College, Hanover, NH 03755-3571, USA

*Corresponding author.

E-mail address: annaksch@gmail.com (A. K. Schartman).

Declaration of interests: none.

Keywords: Leaf wax; Hydrogen isotopes; Holocene; Late glacial; North America; Organic geochemistry; Paleoclimatology; Precipitation sourcing

Highlights:

(1) Organic matter source shifts from lacustrine to terrestrial in the earliest Holocene

(2) *n*-Alkane δD values are dependent on lake catchment characteristics

(3) Changes in δD during the late glacial may be due to precipitation or vegetation

(4) During the Holocene, growing season precipitation δD varies by ~22‰

(5) Precipitation δD stability suggests stable synoptic spring atmospheric circulation

Abstract:

Changes in synoptic atmospheric circulation patterns are thought to play a role in establishing millennial scale climate periods during the end of the late glacial and the Holocene. In the northeastern United States, multi-proxy evidence documents fluctuations in effective moisture and temperatures for this time period, but constraining the relationship between atmospheric processes and these climate regimes is not straightforward. Because the hydrogen-isotope ratios of sedimentary terrestrial leaf waxes can reflect precipitation δD, these long-chain hydrocarbon compounds are an excellent tool to investigate moisture sourcing. Here we present lake sediment and leaf wax carbon- and hydrogen-isotope records that span the past ~14.0 thousand years from Heart Lake and Moose Pond in the Adirondack Mountains (ADK), New York. High initial lake productivity after basin inception is reflected in low C:N ratios (< 15), and higher relative short chain *n*-alkane (n-C_{17}, n-C_{19}, and n-C_{21}) to long chain *n*-alkane (n-C_{27}, n-C_{29} and n-C_{31}) concentration ratios. The Holocene record is characterized by low bulk and *n*-alkane $\delta^{13}C$ (~ –28‰, ~ –31‰, respectively), high $ACL_{25\text{-}35}$ (~28), and high relative concentrations of long chain *n*-alkane homologues, indicating a dominantly terrestrial source of organic matter for this time period. Hydrogen-isotope ratios of n-C_{29} *n*-alkane from both lake basins range only ~20‰ through the Holocene and reconstructed precipitation δD (δD_{precip}) from both basins is in good agreement with that of modern modeled spring precipitation. This suggests there may have been no major changes in the sourcing of spring precipitation for the ADK throughout the time of record.

1. Introduction

Atmospheric circulation dynamics are a key component of a region's climate system, but how these dynamics are integrated into past hydroclimate regimes remains a challenge to constrain. In the northeastern United States (here defined as New England and the upper Mid-Atlantic states of Pennsylvania, New York and New Jersey), the end of the late glacial and the Holocene Epoch are a time of well-documented millennial-scale variability in temperatures and effective moisture (e.g. Cwynar and Spear, 2001; Foster et al., 2006; Hou et al., 2012; Hubeny et al., 2011; Kirby, Patterson, Mullins & Burnett, 2002; Kirby, Mullins, Patterson & Burnett, 2002; Marsicek et al., 2013; McFadden et al, 2005; Menking et al., 2012; Newby et al., 2009; Oswald et al., 2018; Shuman and Marsicek, 2016; Yu, 2000; C. Zhao et al., 2010; Y. Zhao et al., 2010). Because air mass source and trajectory can greatly influence regional temperatures, precipitation amount and seasonality (e.g. Amini and Straus, 2019; Fukushima et al., 2019; Xu et al., 2019), it is possible that there is a relationship between late glacial and Holocene atmospheric circulation patterns and the hydroclimate variability observed in these proxy records (e.g. Gao et al., 2017; Hubeny et al., 2011; Kirby, Mullins et al., 2002; Liu et al., 2014; Shuman et al., 2006; C. Zhao et al., 2010). Proxy records that document air mass source evolution can therefore provide insight into the significance of this relationship for sites in the northeastern United States from the end of the late glacial through the Holocene.

In order to understand past atmospheric circulation variability, hydrogen isotopes of terrestrial leaf waxes preserved in sediments have been used increasingly in recent years (e.g. Bhattacharya et al., 2018; Feakins et al., 2019; Thomas et al., 2016; Tierney et al., 2010). In the modern, leaf wax compounds have been shown to record the δD of the growth water the plant used during biosynthesis of these compounds. For terrestrial plants in temperate environments such as the northeastern United States, the growth water is the water available in the soil column during the time of leaf wax synthesis and production, and largely reflects δD of precipitation (Freimuth et al., 2020; Sachse et al., 2012 and references therein). The hydrogen isotopes of sedimentary leaf waxes for a temperate forest environment should therefore track precipitation δD through time, having the potential to record changes in hydroclimate due to atmospheric circulation reorganization (e.g. Rach et al., 2014).

Here we use terrestrial leaf wax biomarkers extracted from the sediments of two lakes in the Adirondack Mountains (ADK) of upstate New York in order to evaluate precipitation source trends from the end of the late glacial through the Holocene for the northeastern United States. The modern climate of the ADK is influenced by the Pacific North American (PNA) and North American Oscillation (NAO) teleconnection patterns, as documented by correlation between these indices and, for example, monthly streamflow (Bradbury et al., 2002), winter snowfall totals (Hartley and Keables, 1998), and remote sensing wavelet analysis of precipitation and greenness (Mullon et al., 2013). The ADK also has been demonstrated to receive moisture seasonally from a variety of sources with dissimilar isotopic signals (Burnett et al., 2004; Puntsag et al., 2016). Thus, this site is ideally located to provide sediment records sensitive to shifts in atmospheric circulation patterns and concomitant changes in precipitation source. Furthermore, a wealth of previous studies conducted in the ADK investigating paleoecology (e.g. Jackson, 1989; Jackson and Whitehead 1991; Lavoie et al., 2015; Overpeck, 1985; Whitehead and Jackson, 1990; Whitehead et al., 1989), lake development and acidification (e.g. Arseneau et al., 2016; 2011; Driscoll et al., 2016; Driscoll and Newton, 1985; Whitehead et al., 1989), soil chemistry (e.g. April et al., 2004; April and Newton, 1983; Sullivan et al., 2006; Zarfos et al., 2019) and modern leaf wax taphonomy and incorporation into lake sediments (Freimuth et al., 2020) aid in the interpretation and contextualization of the downcore leaf wax record. Finally, evaluating the two lake records in tandem will allow us to better deconvolve the signal of precipitation sourcing through time from other catchment specific influencing factors, to determine if atmospheric circulation patterns have shifted in step with other late glacial and Holocene climate variables, or if these patterns have remained largely continuous throughout the time of record.

2. Background and Study Site

The Adirondack Mountains of northeastern New York comprise a 24,000 km^2 geologic dome of Proterozoic origin, heavily dissected in the late Quaternary by continental ice during the last glaciation (Barth et al., 2019; Craft, 1979; Isachsen and Fisher, 1970). Total elevation within the ADK ranges from 37 m to 1,629 m above sea-level with the highest peaks occurring in the central to northeast section of the mountain range where both of the study lakes are located (Figure 1). There are approximately 2,800 lakes covering more than 1,000 km^2 distributed throughout the ADK, many of which formed as the region deglaciated prior to 13.0 cal kyr BP (Barth et al., 2019; Driscoll et al., 1991).

The modern climate of the Adirondacks is humid-continental, having cool summers and cold winters (Peel et al., 2007) with precipitation amounts increasing from the northeast to southwest across the mountain range (Ito et al., 2002). Climate normal datasets from National Weather Service stations within a 50 km radius of either study site and for the years 1981 – 2010 record an average mean annual temperature between 4.2 and 6.8°C, while the average mean annual precipitation amounts ranged from 948 to 1,138 mm (Arguez et al., 2010). The same climate normal datasets record precipitation minima occurring in winter (DJF: 213 mm), and maxima occurring in summer (JJA: 309 mm). Spring (MAM; 243 mm) and fall (SON: 290 mm) seasons have intermediate values (Arguez et al., 2010). There are marked altitudinal gradients within the ADK so that temperature decreases, and cloud cover, wind velocity and precipitation increase with increasing elevation (Ito et al., 2002; Miller et al., 1993; Schlesinger and Reiners, 1974). Snowfall occurs throughout the months of October through May and lake effect snowfall is a contributor to winter precipitation totals with importance diminishing rapidly to the east (Veals and Steenburgh, 2015).

The dominant air masses that contribute precipitation throughout the year to the ADK are (1) dry northern and continental air, (2) moist southern air originating in the Gulf of Mexico and South Atlantic, and (3) moist coastal air from the North Atlantic (Bryson and Hare, 1974; Burnett et al., 2004; Puntsag et al., 2016). The hydrogen and oxygen isotopic values of precipitation as well as moisture content varies by air mass source and trajectory (Burnett et al., 2004; Figure 2). Generally, northern continental sources are the driest and contain the most negative $\delta^{18}O$ and δD precipitation values. Atlantic coastal systems produce the greatest amounts of precipitation having intermediate isotope values, while southern sourced air masses contribute intermediate amounts of precipitation but are the most positive. For example, over a five-month period (November through March), precipitation isotope measurements conducted in Hamilton, New York, revealed an average oxygen-isotope composition of –17.9‰ and average hydrogen-isotope composition of –127‰ for northern continental sources. Southern sourced air masses produced the most positive average oxygen (–8.2‰) and hydrogen (–52‰) isotope values, while Atlantic coastal systems' precipitation averaged –16.1‰ for $\delta^{18}O$ and –113‰ for δD (Burnett et al., 2004; Figure 2).

The ADK is located in the eastern North American temperate broadleaf and mixed forest biome (Olson et al., 2001). Within the mountain range, the modern vegetation zones primarily reflect differences in elevation (Jackson, 1989; Jackson and Whitehead, 1991; Overpeck, 1985; Whitehead et al., 1989). While northern hardwood-conifer forest is predominant at low elevations (< 300 m), mixed conifer-northern hardwood, subalpine spruce-fir-paper birch, and subalpine fir forest become the dominant forest type at progressively higher elevations (Jackson, 1989; Whitehead et al., 1989). The Adirondacks have been forested beginning from ~11.9 to ~9.6 cal kyr BP, and modern vegetation assemblages were established by ~2.0 to ~1.0 cal kyr BP (Lavoie et al, 2015; Jackson, 1989; Overpeck et al., 1985; Whitehead et al., 1989; Whitehead and Jackson, 1990). Prior to forest establishment, the vegetation assemblage has been characterized as non-arboreal shrub tundra (Lavoie et al., 2015) or as matching most closely to modern and forest-tundra (Whitehead and Jackson, 1990).

The two study sites, Heart Lake (44.18°N, 73.97°W) and Moose Pond (44.37°N, 74.06°W), are located in the central-northeast of the ADK within the mixed conifer-northern hardwood vegetation zone, and approximately 25 km distant from each other (Figure 1). Heart Lake is a small (0.1 km^2), oligotrophic lake with a maximum depth of 14 m occupying a depression between two local peaks (Figure 3A). The lake itself is located in the High Peaks region of the Adirondack park at ~665 m, in a small catchment (~1 km^2) of minimal elevation range (~ 200 m; Freimuth et al., 2020). The lake has a single depocenter, which is the coring location for this study (Figure 3A). There are no continual inlets and only one outlet which drains the lake to the southeast (Freimuth et al., 2020; Jackson, 1989). In comparison, Moose Pond is outside the High Peaks region, at lower elevation (475 m), of larger size (0.7 km^2), has a greater maximum depth (22 m), and much larger catchment area (~17 km^2; Figure 3B). Furthermore, Moose Pond has a greater degree of hydrological and morphometric complexity (Figure 3B). The northeast inlet connecting Moose Pond to an upstream wetland area has formed a pro-grading delta into Moose Pond adjacent to the coring location. Because the Moose Pond catchment contains the northern flanks of McKenzie Mountain, total elevation range within the catchment (~ 700 m) is greater than at Heart Lake. The relevant hydrologic and topographic information for each basin and catchment is summarized in Table 1.

3. Materials and Methods

3.1 Bulk sediment retrieval and analysis

Sediments were sampled at Heart Lake and Moose Pond in February 2017 using a Livingstone square-rod piston coring device. At both sites two adjacent cores were recovered offset in depth by ~50 cm. All cores were wrapped in plastic wrap, stored in PVC tubing, and removed to the University of Cincinnati and St. Lawrence University. They were then split, described, and subsampled for loss-on-ignition, magnetic susceptibility, grain size, bulk sediment, lipid and radiocarbon analysis. Loss-on-ignition sampling was conducted at 4-cm intervals and combusted at 550°C (4 hr) and 1000°C (2 hr) for total wt. % organic matter (TOM) and total carbonate (TC) respectively (Heiri et al., 2001; Shuman, 2003). To assess magnetic susceptibility, all cores were scanned with a Bartington MS2 meter at 2 cm resolution. Subsamples were taken for grain size analysis at every 20 cm, then pre-treated following the methods of Gray et al. (2010) and Bird et al. (2014). A Beckman-Coulter LS230 instrument was used to determine the particle distribution, as described in Freimuth et al. (2020).

Bulk sediment total organic carbon (TOC), total nitrogen (TN) and $\delta^{13}C$ organic were determined from decarbonized, dried and homogenized aliquots of 20 cm resolution using the methods of Diefendorf et al. (2008) on a Costech elemental analyzer interfaced with an IRMS via a Conflo IV. C:N ratios were calculated from the ratio of wt. % TOC to wt. % TN. $\delta^{13}C$

organic values were normalized to the VPDB scale after correction for sample size dependency (Coplen et al., 2006) and a precision of 0.07‰ (1σ, n = 65) and accuracy of 0.07‰ (1σ, n = 12) were calculated using four independent laboratory standards.

3.2 Biomarker analysis

Sediment samples of ~1.5 cm^3 were retrieved from Heart Lake and Moose Pond cores at ~40 cm resolution for compound-specific hydrogen- and carbon-isotope analysis. All samples were first freeze-dried and homogenized. The total lipid extract (TLE) was produced by accelerated solvent extraction on a Dionex 350 with 5:1 (v/v) DCM/MeOH. Half the TLE was archived while the working half was separated by activated alumina oxide column chromatography into aliphatic and polar fractions. Unsaturated and saturated compounds were separated from the aliphatic fraction using 5% silver silica gel and eluting with hexanes (Freimuth et al., 2020). Identification of *n*-alkanes was completed on a GC-MS using an Agilent 7890A GC and Agilent 5975C quadrupole mass selective detector. A fused silica column (Agilent J&W DB-5ms; 30 m x 0.25 mm, 25 µm film) was used for separation. Compounds were identified by comparison of mass spectra to published spectra, comparison to standards (*n*-alkanes C_7 to C_{40}; Supelco, Bellefonte, USA), and by retention time. For quantitation, samples were spiked with an internal standard (1,1'-binaphthyl; 25 µg/ml) before quantification on the same GC-MS with a flame ionization detector (FID). The internal standard was used to normalize the compound peak areas and, with the response curves of *n*-alkane standards (C_7 to C_{40}), converted to concentration. Precision (0.61, 1σ , n = 16) and accuracy (0.41, 1σ, n = 16) were determined from the analysis of external standards at 25 µg/ml. All concentrations were normalized to the mass of dry sediment extracted. For samples containing an unresolved complex mixture (UCM) or coelution of *n*-alkanes with other compounds, urea adduction was performed after quantitation and prior to isotope analysis. Branched/cyclic compounds were separated by adducting *n*-alkanes in urea crystals with equal parts 10% urea in methanol (w/w), acetone, and *n*-pentane by freezing and subsequent evaporation with nitrogen. Non adducts were extracted with hexanes. and urea crystals were subsequently dissolved with water and methanol to release *n*-alkanes and then liquid-liquid extracted with hexanes.

We calculated the weighted average concentration of all long chain *n*-alkanes (ACL) for each sample using the chain lengths *n*-C_{25} through *n*-C_{35} and defined as:

Equation 1:

$$\mathrm{ACL}_{25-35} = \frac{(25[\mathrm{C}_{25}] + 27[\mathrm{C}_{27}] + 29[\mathrm{C}_{29}] + 31[\mathrm{C}_{31}] + 33[\mathrm{C}_{33}] + 35[\mathrm{C}_{35}])}{([\mathrm{C}_{25}] + [\mathrm{C}_{27}] + [\mathrm{C}_{29}] + [\mathrm{C}_{31}] + [\mathrm{C}_{33}] + [\mathrm{C}_{35}])}$$

where the square brackets indicate the concentration of each homologue in µg/g dry sediment present in a sample. Carbon preference index (CPI) values measuring the relative abundance of odd over even carbon chain lengths for each sample were also calculated as follows (Marzi et al., 1993):

Equation 2:

$$\mathrm{CPI} = \frac{[\Sigma_{\mathrm{odd}}(\mathrm{C}_{21-33}) + \Sigma_{\mathrm{odd}}(\mathrm{C}_{23-35})]}{2\Sigma_{\mathrm{even}}(\mathrm{C}_{22-34})}$$

Samples with CPI values greater than one have a higher contribution of odd chain lengths (21 through 35) than even chain lengths (22 through 34), which is taken as a possible indication of a terrestrial plant source (Eglinton and Hamilton, 1967).

Gas chromatography isotope ratio mass spectrometry (GC-IRMS) was used to determine *n*-alkane hydrogen and carbon isotopic composition. We used a Thermo Trace GC Ultra equipped with an Isolink pyrolysis reactor (at 1420°C) interfaced with a Thermo Electron Delta V Advantage IRMS via a Conflo IV for measurement of δD. For $\delta^{13}C$, an Isolink combustion reactor (at 1000°C) replaced the pyrolysis reactor. Details of GC conditions and instrumentation are provided in Freimuth et al. (2020). The isotopic composition of samples was normalized to the VSMOW/VSLAP or VPDB scale using periodic interspersed standards of known δD and $\delta^{13}C$ composition (Mix A6, A. Schimmelmann, Indiana University) and are reported in standard delta notation. We determined the analytical precision to be 3.1‰ for δD by pooling the standard deviation from all replicate sample measurements following Polissar and D'Andrea (2014). The precision on the co-injected *n*-C_{38} internal standard for all samples and standards is 3.6‰ ($\sigma = 1$, $n = 110$) for δD and 0.31‰ ($\sigma = 1$, $n = 140$) for $\delta^{13}C$.

3.3 Age Models

3.3 Age Models

Independent age models were constructed for Heart Lake and Moose Pond based on radiocarbon dates for organic terrestrial macrofossils, and sediment ^{210}Pb ages. Samples for radiocarbon analysis were removed from cores, cleaned under stereomicroscope, dried at 60°C, and sent to the National Ocean Sciences Accelerator Mass Spectrometry (NOSAMS) facility for ^{14}C analysis (Table 2). Samples for ^{210}Pb analysis were taken from surface sediment cores that were collected from the same coring location as this study and described in Freimuth et al. (2020). Briefly, one half of each split surface core was sub-sampled for ^{210}Pb dating at 0.5 – 2 cm wide intervals from the top of the core to the depth at which unsupported (excess) ^{210}Pb was no longer measurable (99 cm at Heart Lake and 37 cm at Moose Pond). Lake sediment chronologies for the surface sediment cores were established at the Dartmouth GeoAnalytical Resource Center, in Hanover, New Hampshire, using ^{210}Pb dating and the Constant Rate of Supply (CRS) model (Appleby and Oldfield, 1978). Total ^{210}Pb for each core depth interval ($^{210}Pb_T$) was measured by gamma spectrometry using Canberra well-type and broad-energy intrinsic Ge detectors, and instrument calibration was performed using matrix-matched calibration standards of lake sediments mixed with 1% (w/w) reference uranium ore BL-5 (Canadian Certified Reference Material Project, Ottawa). The atmospheric or excess ^{210}Pb component ($^{210}Pb_{xs}$) required for the CRS model was calculated as $^{210}Pb_T$ for each depth interval minus a uniform supported ^{210}Pb activity for each core. Supported ^{210}Pb activity was taken as the convergence of the $^{210}Pb_T$ asymptote with ^{226}Ra activity for the core, was estimated as a variance-weighted mean of the two measures, and ranged 10-14 Bq kg^{-1}. For each interval ^{226}Ra was measured at 186 keV (with deconvolution from ^{235}U) and confirmed with surrogates ^{214}Pb (295 and 352 keV) and ^{214}Bi (609 keV). Cumulative analytical uncertainties were propagated as described by Landis et al. (2012), and age model uncertainties were propagated following Binford (1990). The Heart Lake and Moose Pond ^{210}Pb age model data is reported in full in the Appendix, Table A.1 and A.2. Surface sediment cores were then correlated with the Livingston piston cores by field observations, collection depth information, and curve matching of loss-on-ignition data. As no samples for chemical analysis reported in this study were taken from the surface sediment cores, they are not described in any further detail here.

To generate the chronology for each lake's Livingston sediment core, we employed Bayesian age-depth modeling techniques (Bacon v2.2; Blaauw and Christen, 2011) using the most recent calibration curve, IntCal 13 (Reimer et al., 2013). We accepted the default values for input parameters relating to the accumulation rate (acc.mean; acc.shape) and memory properties (mem.mean; mem.strength) for all models (Blaauw and Christen, 2011). To capture the age-depth relationship near the sediment water interface, and in order to keep age models consistent with previous and future publications, we integrated into our models the ^{210}Pb ages from surface sediment cores described above. To correlate the Heart Lake sediment core and chemical analysis reported here with a palynological record of Heart Lake reported in Whitehead and Jackson (1990), we generated an updated age-depth model for the previously published record using Bacon v2.2 and IntCal 13 as described above. The two Heart Lake core records were then correlated with each other by age. The resulting age-depth relationships are shown in Figure 4, and the original Bacon output plots are included in the Appendix, Figure A.1. All ages are reported in cal yr BP where 0 cal yr BP is 1950 AD, and rounded to the nearest 0.1 cal kyr BP.

4. Results

The stratigraphic sections, bulk chemistry and isotope analyses of Heart Lake and Moose Pond provide information into the paleolimnological development of the two basins from lake inception after deglaciation to the modern day (Figures 5 and 6). Because both study sites are similar in stratigraphy, bulk sediment chemistry and compound-specific isotope analysis, we will structure the following section by analysis result as opposed to study site in order to better highlight where the two records agree and where discrepancies arise. All data are included in Appendix A.

4.1 Stratigraphic Sections and Age Models

The Heart Lake cores are dominantly composed of massive dark-brown silts rich in aquatic and terrestrial macrofossils (Unit A) or barren (Unit B), with an underlying basal unit of alternating glacially derived barren silts and sands (Unit C; Figure 5A). The Moose Pond cores also contain three distinct units (Figure 6A). The uppermost (Unit A) is dominantly composed of micaceous black-brown silts with abundant macrofossils, which transitions into light-grey, barren silts (Unit B). As at Heart Lake, the Moose Pond cores have a basal unit of alternating barren silts and sands (Unit C). The silts and sands of Unit C were likely deposited immediately following glacial retreat and therefore we assume this unit has sedimentation rates greater than the upper two units. High sedimentation rates are not unexpected over this interval and are reported elsewhere for glacially derived lakes with similar stratigraphic units (e.g. Crann et al., 2015). As sediment availability is high immediately following ice-sheet retreat, and can be rapidly deposited into lake basins due to lack of vegetation, lakes occupying post-glacial environments like Heart Lake and Moose Pond are therefore known to have elevated sedimentation rates at the beginning of record (e.g. Ballantyne, 2002 and references therein; Chang Huang et al., 2004; Church and Ryder, 1972).

The oldest calibrated age for Heart Lake (12.0 cal kyr BP) and Moose Pond (13.4 cal kyr BP) occurs at the base of Unit B (65 cm from the base of the core) and the middle of Unit C (54 cm from the base of the core) respectively. All samples below these limiting ages and depths are sourced from the sand dominated Unit C of each lake and are interpreted only in reference to their stratigraphic position (Figure 4). The oldest calibrated age for the Heart Lake core of Whitehead and Jackson (1990) is reported in that study as 10,475 ± 230 yrs BP. The remodeled age using Bacon v2.2 (see Section 3.3) is 11.0 cal kyr BP. This age corresponds to a sample located stratigraphically ~70 cm from the core's base at the top of Unit B. Despite differences in the total lengths of Units A, B and C within the two Heart Lake records, the age models produce unit boundaries for each core that match within ~600 years (Figure 4). In general, the age model produced from the Whitehead and Jackson (1990) data is older for a given depth than the Heart Lake age model reported in this study. However, this age offset decreases with increasing depth, and by ~4.2 cal kyr BP, the 95% confidence intervals of both age models overlap.

As Unit C displays features of rapid sedimentation in both the Heart Lake and Moose Pond records, we speculate that sampling intervals for compound-specific and bulk sediment analysis throughout this unit represent time frames on the order of 10s to several 100s of years at the maximum. Further, due to the sudden change in sedimentation between Unit C and the overlying Unit B evident in the stratigraphy, and the sparse age controls from these depths, the age models may not capture the sedimentation rate through this interval well. Given these limitations, the exact timing of the initiation of lacustrine sedimentation for either basin is unknown. However, the deepest radiocarbon samples retrieved from each lake core record provide minimum ages for the beginning of deposition, and are in agreement with the hypothesized timing of deglaciation for the ADK (Barth et al., 2019; Craft, 1979).

4.2 Bulk Sediment Characteristics

Loss-on-ignition analysis reveals low TC values at both Heart Lake and Moose Pond throughout the entirety of the record, averaging only 3.5% in Heart Lake and 0.7% in Moose Pond, and in contrast to TOM, do not show a correlation with unit boundaries. Heart Lake TOM values in Unit C are $< 1.5\%$, increase slightly to $< 12.0\%$ in Unit B, and range between 27.5% and 53.1% for Unit A (Figure 5B). Overall the inorganic component of the Moose Pond cores is greater than that of Heart Lake (Figure 6B). TOM values are always $< 36\%$ and generally lowest

(< 3.0%) in the basal unit. Unit B TOM values increase slightly from Unit C to an average of 4.1%, and increase again to an average of 17.3% in Unit A. The greater size of Moose Pond, and the presence of the inlet and associated delta near to the coring location (Figure 3B), may have allowed greater total deposition of inorganic relative to organic material at this site as evidenced in the lower TOM values compared to Heart Lake (Figures 5B, 6B).

C:N ratios are stable over the majority of the Heart Lake record, remaining between values of ~13 and ~17 and indicating a mixed contribution of vascular and aquatic sourcing of the sedimentary organic material (Meyers, 2003; Meyers and Lallier-Vergès, 1999; Figure 5C). Lowest values of ~13 occur in Unit C, likely indicating a higher contribution of aquatic sourced carbon during the deposition of this unit. Bulk sedimentary $\delta^{13}C$ organic values are likewise stable over the majority of the record, averaging –28.1‰ (σ = 0.4‰, n = 37) in Unit A, while values are consistently ~ 3‰ more positive throughout Unit C (Figure 5D). Moose Pond C:N ratios are overall higher than at Heart Lake, averaging ~17 throughout the record, and therefore likely indicating a greater relative component of terrestrial organic carbon flux into the lake basin (Figure 6C). As at Heart Lake, the lowest C:N values (~13) are also found in the basal unit. $\delta^{13}C$ organic values are stable in Units A and B with an average value of –27.8‰ (σ = 0.4‰, n = 32), contrasting slightly with Unit C where the values are again more positive (~ –26‰; Figure 6D).

Magnetic susceptibility is low (~ 0 CGS units) throughout Units A and B at Heart Lake, peaking at 0.007 CGS units at the very base of Unit C (Figure A.2 A). Moose Pond has slightly higher basal values (0.009 CGS Units) which decreases gradually to ~ 0 CGS units by the base of Unit A (Figure A.2 A). Grain size distributions show no systematic change between units potentially due to the low sampling resolution (Figure A.2 B).

4.3 Biomarker Analysis

4.3.1 *n*-alkane concentration

We identified *n*-C_{16} through *n*-C_{35} *n*-alkanes at Heart Lake and Moose Pond (Figures 5E and 6E). At Heart Lake, concentrations of all *n*-alkanes are lowest in Unit C (< 0.4 µg/g). Alkanes *n*-C_{23} through *n*-C_{31} increase in Unit B (< 2.4 µg/g) and rise in Unit A to concentration peaks between 11.0 and 8.5 cal yr BP, where *n*-C_{27} and *n*-C_{29} reach maximum concentrations (41.3 µg/g and 37.0 µg/g, respectively; Figure 5E). The short-chain homologues (*n*-C_{17} , *n*-C_{19} and *n*-C_{21}), however, remain in low concentrations throughout. There is a strong odd over even preference throughout the Heart Lake record which supports the interpretation of organic matter sourcing from terrestrial vegetation (e.g. Eglinton and Hamilton, 1967). Carbon preference index (CPI) values always remain above one (mean = 6.0, σ = 0.9, n = 29 ; Figure A.3 A). The dominant homologues are *n*-C_{27} and *n*-C_{29} throughout the entirety of the record excepting the base of Unit C where shorter chain homologues (*n*-C_{17} to *n*-C_{23}) are the most abundant (Figures 5E; A.4). A pronounced shift from *n*-C_{27} to *n*-C_{29} at ~8.5 cal kyr BP occurs, likely reflecting a change in terrestrial vegetation composition within the catchment (Figure 5E). The average chain length (ACL), calculated as the average value of the abundance of chain lengths *n*-C_{25} through *n*-C_{35}, is also consistent with values for higher terrestrial plants at 28.4 (σ = 0.5, n = 29; Diefendorf and Freimuth, 2017; Eglinton and Hamilton, 1967; Ficken at al., 2000; Figures A.3 B and 5F).

Like Unit C of Heart Lake, total *n*-alkane concentrations in Unit C of Moose Pond are similarly low (< 1.3 µg/g) as are those found in Unit B (< 1.5 µg/g; Figure 6E). Concentrations of long-chain homologues (*n*-C_{27}, *n*-C_{29} and *n*-C_{31}) rise in Unit A. In this unit *n*-C_{27} and *n*-C_{29} reach their highest values (7.8 µg/g and 7.4 µg/g, respectively). The lower total concentration of *n*-alkanes at Moose Pond compared to Heart Lake is consistent with the lower TOM values described in Section 4.2 (Figure 6B). Unlike at Heart Lake, n-C_{27} is in greater concentration throughout the majority of the record at Moose Pond, although actual concentrations of n-C_{27} and n-C_{29} are similar (Figure 6E; Figure A.4 D). CPI values at Moose Pond show the odd over even preference with an average value of 8.2 ($\sigma = 2.6$, n = 31), while ACL values are stable and average 28.3 ($\sigma = 0.3$, n = 31), both suggesting a terrestrial source of organic carbon for the basin (Figures A.3 A, A.3 B, and 6F).

4.3.2 $\delta^{13}C$ of n-alkanes

We measured the carbon isotopic composition of four chain lengths (n-C_{25}, n-C_{27}, n-C_{29}, and n-C_{31}) and report all values (see the Appendix, Table A.3 and Figure A.5 A). At a first order, all chain lengths display little variation and have very similar ranges throughout the record for both Heart Lake (mean = –30.2‰, $\sigma = 0.9$, n = 110) and Moose Pond (mean = –30.8‰, $\sigma = 0.6$, n = 116). Because n-C_{29} and n-C_{27} are of greater concentration throughout the majority of the record, we will focus the following discussion on these two chain lengths. The average $\delta^{13}C$ values of ~ –30‰ and small ranges of n-C_{29} and n-C_{27} are consistent with a stable terrigenous source of vegetation for both study lakes (Diefendorf and Freimuth, 2017; Figure A.5 A). At a second order, Heart Lake and Moose Pond display most negative n-C_{29} values (–32.8‰ and –32.6‰, respectively) in Unit C at the base of the record, before stabilizing at ~ –30‰. The n-C_{27} values are likewise the most negative in Unit C of Heart Lake and Moose Pond (both –31.4‰), but the most positive values (–27.4‰, and –29.2‰, respectively) found within the record occur in this unit as well (Figure A.5 A). The shift from most negative to most positive values in the rapidly deposited Unit C of both lake basins is interpreted as an indication of a change in the composition of sources of sedimentary organic matter to the lake sites.

4.3.3 δD of *n*-alkanes

We report the hydrogen isotopic composition of four chain lengths for which compound abundances allowed for consistent measurement (*n*-C_{25}, *n*-C_{27}, *n*-C_{29}, and *n*-C_{31}), and plot the results for *n*-C_{27} and *n*-C_{29} in Figure 7 (for all values see the Appendix, Table A.3, and Figure A.5 B). At Heart Lake δD *n*-C_{27} values (δD_{27}) of Unit C range over 19.7‰ from a minimum of –167.4‰ to a maximum of –147.7‰ in the most basal sample (Figure 7B). The δD of *n*-C_{29} (δD_{29}) found in Unit C has a total range of 38.6‰, while the minimum and maximum values are –173.6‰ and –135.0‰ respectively. More negative values and smaller ranges are seen at Moose Pond for the same unit (Figure 7A). δD_{27} ranges a total of 28.9‰ from –188.6‰ to –159.7‰, while δD_{29} has a minimum of –185.8‰, a maximum of –171.5‰ and total range of only 14.4‰. For both Heart Lake and Moose Pond, *n*-alkane δD_{27} and δD_{29} are consistent through Units A and B, represented by their small ranges (Figures 7A and 7B). At Heart Lake, δD_{27} has a minimum of –196.6‰, a maximum of –178.4‰ and a total range of 18.3‰ throughout these two units. The minimum and maximum of δD_{29} is –183.1‰ and –166.1‰ respectively, and total range is only 17.0‰ (Figure 7B). Moose Pond has a δD_{27} range through Units A and B of 23.3‰, a minimum of –194.4‰ and maximum of –171.1‰ (Figure 7A). The δD_{29} range is 18.4‰, while the minimum and maximum values are –188.4‰ and –170.0‰, respectively (Figure 7A). In sum, the same major trend is observed in both lake records. In Unit C, δD_{27} and δD_{29} become progressively more negative up-core, before stabilizing in Units A and B and exhibiting much-decreased variability throughout this interval.

We use δD_{29} for paleoclimate reconstructions as higher chain lengths (*n*-C_{29}, *n*-C_{31}) are interpreted as sourced most reliably from terrestrial vascular plants (Diefendorf and Freimuth, 2017; Sachse et al., 2012). In order to reconstruct precipitation hydrogen-isotope values (δD_{precip}), it is necessary to have an estimate of the net apparent fractionation (ε_{app}) between the measured sedimentary leaf wax δD (δD_{29}) and the paleoprecipitation hydrogen-isotope composition. To generate δD_{precip} from δD_{29}, we used an ε_{app} of –123‰, calculated for the modern ADK and reported in Freimuth et al. (2020). We note that this value is in good agreement with the ε_{app} of temperate forest environments suggested by other authors of –131‰ through –137‰ (Polissar and Freeman, 2010; Sachse et al., 2004; Seki et al., 2010). δD_{precip} was calculated using the following equation and is reported in values ‰:

Equation 3:

$$\delta D_{precip} = \left[\frac{\delta D_{29} + 1}{\varepsilon_{app} + 1}\right]$$

We plot δD_{precip} for Heart Lake and Moose Pond in Figure 7C. Average late glacial δD_{precip} at Heart Lake is –45.8‰, but the variability is high ($\sigma = 21.5$‰, n = 4). In contrast, the late glacial δD_{precip} values from Moose Pond average –65.9‰ and exhibit less variability ($\sigma = 6.6$‰, n = 9). Average Holocene values for Heart Lake are –61.1‰ ($\sigma = 5.4$, n = 25) while at Moose Pond the Holocene average is slightly more negative (mean = –66.1‰, $\sigma = 5.8$, n = 22). At 5‰, the Holocene difference in δD_{precip} between Heart Lake and Moose Pond is significant, although small (t-test, $p = 0.004$).

In sum, the bulk chemical and *n*-alkane $\delta^{13}C$ data are congruous between both lake records, as are the first order *n*-alkane δD and concentration data. We will use these chemical analyses records to motivate a similar developmental history for both Heart Lake and Moose

Pond. However, as the compound-specific concentration and hydrogen-isotope profiles are not identical, we will also attempt to tease apart causes of these differences in the following sections.

4.3.4 Modern ADK Hydrologic and Sediment Isotope Records

In order to evaluate the ADK hydroclimate reconstruction from Heart Lake and Moose Pond presented here, we compare it to modern precipitation, surface water, xylem water and surface sediment isotopic data (Figure 8). Because a long-term record of precipitation isotopes is not available at the two study sites, we use the Online Isotope in Precipitation Calculator (OIPC; Bowen, 2018; Bowen and Revenaugh, 2003) to model monthly precipitation δD and $\delta^{18}O$ for the ADK (Figure 8). Using this approach, Freimuth et al. (2020) calculated a regional meteoric water line (RMWL) for the ADK based on OIPC values for 12 study sites, including Heart Lake and Moose Pond. Additionally, they incorporated 87 water samples from 42 sites in the ADK to develop a regional evaporation line (REL). The interception of the REL with the RMWL defines mean annual precipitation isotope values (δD_{MAP} and $\delta^{18}O_{MAP}$) for a location (Beria et al., 2018; Henderson et al., 2009). For the region, δD_{MAP} is –77‰. In temperate forest environments, sedimentary *n*-alkane δD is often considered representative of δD_{MAP} offset by the apparent fractionation (ε_{app}) between the leaf wax compounds and precipitation (Sachse et al., 2012 and references therein). However, other authors have found evidence that the hydrogen-isotope signal is biased towards spring precipitation events, as this is the time of greatest leaf wax synthesis (Freimuth et al., 2017; Kahmen et al., 2011; Sachse et al., 2010; Tipple et al., 2013).

For the ADK, the δD ratios of the xylem water samples are not consistent with average modeled May precipitation δD, the month of collection, being on average ~30‰ more negative (Freimuth et al., 2020; Figure 8). As the averaged xylem water samples are also ~10‰ more negative than the modeled April precipitation δD values, the soil water likely integrates precipitation over time frames greater than a few months, either directly from precipitation events or through some amount of springtime snowmelt. However, given that the spring precipitation isotope value of –74‰ (here determined as the averaged OIPC δD ratios for the months of March, April and May) is minimally offset from that of mean annual precipitation, we cannot determine from the data whether the May xylem water samples are representative of spring precipitation or are integrated over the entire year (Figure 8). Surface sediment data collected from all 12 lake sites are equally inconclusive, as δD_{precip} from sediments sampled at 1 cm from each lake ranges from –86.5‰ to –63.0‰ (Freimuth et al., 2020). This range (23.5‰) is approximately the total Holocene range observed at Heart Lake (22.1‰) and Moose Pond (23.1‰). Here we will follow the work of Freimuth et al. (2017), Kahmen et al. (2011) and Tipple et al. (2013) and interpret the reconstructed δD_{precip} from the Heart Lake and Moose Pond sediment records as weighted towards spring precipitation δD, the timing of leaf flush.

5. Discussion:

5.1 Basin Development

The chemical, stable isotope, and radiocarbon records constructed from the Heart Lake and Moose Pond sediment cores demonstrate the developmental history of each basin. The age models of Heart Lake and Moose Pond constrain the timing of initial lacustrine sedimentation for both lakes to sometime during the end of the late glacial (Figure 4). However, due to the lack of age control at the very base of both cores, we are unable to correlate the two lake records with each other by age for those samples which are older than 12.0 cal kyr BP. Briefly, we believe that there are two primary interpretations of this correlation that seem most likely. The first assumes both lake catchments deglaciated at roughly the same time interval and the samples taken from Unit C of both lake records (or those which occur below 12.0 cal kyr BP at Heart Lake and 13.4 cal kyr BP at Moose Pond) are of a similar age. This interpretation necessitates a higher rate of sedimentation for Moose Pond relative to Heart Lake, which is not unlikely given the much larger catchment area of the former relative to the later (Figure 3A and 3B). In contrast, the second interpretation assumes sedimentation rates in the sand dominated Unit C of both lakes were rapid and roughly equal. If this were the case, Moose Pond must have initiated prior to Heart Lake, and samples taken from the Unit C of Moose Pond are likewise older than those taken from the Unit C of Heart Lake. However, it is not possible to conclude with certainty which is the more likely interpretation from the current data. In the remainder of the discussion, we resist speculation as to the correlation between Heart Lake and Moose Pond for those samples which occur below the last calibrated radiocarbon age at each lake and have indicated these age-unconstrained samples on Figures 5,6 and 7.

Regardless of the timing of basin inception, Heart Lake and Moose Pond have similar chemical and isotopic histories through the majority of the record. We will discuss both lakes together in the following sections, treating first with the record for the end of the late glacial (defined here as ~ 14.0 cal kyr BP – 11.5 cal kyr BP), then moving to that of the Holocene (11.5 cal kyr BP – modern). We divided the record into these two time periods based on the visual determination of the chemical analysis data produced for both lake basins as discussed below.

5.2 Lake Inception and Stabilization (~14.0 cal kyr BP to ~11.5 cal kyr BP)

Chemical analysis data suggest a change in carbon sourcing to both lake basins during the end of the late glacial and the transition into the Holocene. The oldest samples from each record indicate organic carbon was contributed from a mixed terrestrial and aquatic source, but remained a small component of the sediment over-all, as substantiated by low wt. % TOM values (Figures 5B and 6B). Aquatic sources for Heart Lake are indicated by greater relative proportions of short chain *n*-alkane homologues (C_{17}, C_{19} and C_{21}), compared to their long chain counterparts (C_{27}, C_{29} and C_{31}), and at Moose Pond are suggested by the high $\delta^{13}C$ bulk sediment values (–19.5‰; Figures A.4 and 6D). On the other hand, the high C:N ratios of the very initial samples at Heart Lake and Moose Pond (16;19), low specific *n*-C_{29} $\delta^{13}C$ values (–32.8‰, –31.4‰), and high ACL_{25} (30, 29) suggest a component of the carbon input that is terrestrial in origin (Figures 5C, 6C, A.5 A and A.3 B).

The palynological and macrofossil studies from the ADK provide insight into the likely sources of this terrestrial carbon through time (Jackson, 1989; Jackson and Whitehead 1991; Overpeck, 1985; Whitehead and Jackson, 1990; Whitehead et al., 1989). These studies consistently find evidence in the oldest portions of their records for high percentages of herbs such as *Cyperaceae* (sedge), *Poaceae* (grass), and the gymnosperms *Picea* (spruce) and *Pinus* (pine), with lower percentages of *Alnus* (alder), *Betula* (birch), *Acer* (maple) and other angiosperm tree taxa (Figure 7D). Whitehead and Jackson, (1990) produced a palynological record for Heart Lake and identified 6 unique vegetation assemblage zones (HP-Zone 1 through HP-Zone 6; Figure 7D). These pollen zones and the associated time intervals over which they occur are one tool to evaluate changes in the chemical analysis data produced in this study. Specifically, we use them here to understand how the *n*-alkane record at Heart Lake is influenced by ecological shifts within the catchment.

HP-Zone 1 is the oldest pollen assemblage zone and is interpreted as representative of a tundra environment. It is composed of ~ 30% *Pinus*, ~ 15% *Picea*, and ~ 25% herbaceous pollen grains, with minor amounts of other taxa such as *Ulmus* (elm), *Salix* (willow), *Quercus* (oak), *Fraxinus* (ash), *Corylus* (hazel), and *Abies* (fir) (Whitehead and Jackson, 1990; Figure 7D). This pollen zone occurs below the last radiocarbon age present in the Whitehead and Jackson (1990) core but, as it is the most basal pollen zone present within the record, it likely overlaps with the basal section of this study's Heart Lake record (Figure 4). Indeed, the results presented here are consistent with a landscape that is undergoing colonization by transient tundra vegetation before shifting to an arboreal dominated assemblage. In particular, the higher ACL values apparent at the base of the Heart Lake record are consistent with those from C_3 grasses and forbs, as are the *n*-C_{31}, *n*-C_{29} and *n*-C_{27} $\delta^{13}C$ values of ~ –31‰ (Diefendorf and Freimuth, 2017 and references therein; Garcin et al., 2014; Figures 5F, A.3 B and A.5 A). High (> 1.0) C_{31}:C_{27} chain-length ratios of the most basal samples provide further evidence, as many modern graminoids and forbs produce greater quantities of *n*-C_{31} relative to *n*-C_{27} than tree species (Diefendorf and Freimuth, 2017 and references therein; Figure A.4 E).

Furthermore, while gymnosperms such as *Picea* and *Pinus* produce orders of magnitude less *n*-alkanes then many of their angiosperm counterparts (Diefendorf et al., 2015; 2011), they are over-represented in pollen records (Schwartz, 1989; Webb et al., 1981). In the ADK, *Pinus* pollen is likely contributed to lake basins from distances greater than 1,000 meters (Jackson, 1990), while the *n*-alkane record is biased towards shoreline and catchment vegetation (Freimuth et al., 2019; 2020). Therefore, herbaceous species of the families *Cyperaceae*, and *Poaceae,* or genera *Ambrosia* (ambrosia), *Artemisia* (wormwood), and *Rumex* (dock), likely make up a greater percentage of catchment vegetation then pollen re-constructions suggest, and potentially are of greater influence on the *n*-alkane sediment signal during this time slice. We interpret this part of the Heart Lake record as representing lake inception directly following ice-melt back when tundra vegetation first colonized the catchment. Because Moose Pond evinces similar chemical analysis data at the base of the record as at Heart Lake, specifically higher ACL values (~29), high (> 1.0) C_{31}:C_{27} chain-length ratios, and compound-specific $\delta^{13}C$ values of ~ –31‰, (Figures 6 F, A.3 B, A.4 E and A.5 A) it is likely that a similar tundra vegetation assemblage was present in this catchment as well. A palynological record for Moose Pond, which is currently not available, would prove this point conclusively.

Furthermore, both the Heart Lake and Moose Pond catchments, although significantly different in size and morphology (Figures 3A and 3B), transitioned rapidly after lake inception until ~11.5 cal kyr BP (Figures 5, 6 and 7). Throughout this interval, wt % TOM values increase progressively, C:N ratios fall to their lowest values, and bulk sediment $\delta^{13}C$ values become more negative (Figures 5B, 5C, 5D, 6B, 6C, and 6D). Vegetation change is also represented in the shifts in C_{21}:C_{29} and C_{23}:C_{29} ratios at both sites (Figure A.4 A and A.4 B). While both ratios decrease initially from the values seen at the base of each record, C_{23}:C_{29} remains elevated at values of ~0.7 until ~10.0 cal kyr BP at Heart Lake and ~11.0 cal kyr BP at Moose Pond (Figure A.4 B). On the other hand, C_{21}:C_{29} remains low throughout the rest of both lake records, providing evidence for a similar sourcing change at both lakes (Figure A.4 A).

The changing chemical characteristics are indicative of catchments undergoing weathering of unconsolidated drift coupled to rapid shifts in vegetation makeup and abundance. Nutrient fluxes to the lake basins increased initially facilitated by the weathering of the recently deglaciated sediments (e.g. Fritz and Anderson, 2013). This encouraged higher rates of lake productivity until ~11.5 cal kyr BP, represented here most strongly in the lower C:N ratios (Figures 5C and 6C). This interpretation is supported by chrysophyte- and diatom- based alkalinity and productivity reconstructions for ADK lakes presented in Whitehead et al. (1989).

These authors find evidence for higher lake productivity at the end of the late glacial which they associate with increased flux of base cations into the lake basins due to the accelerated weathering and erosion processes. This was closely followed by a period of gradual decline in lake water pH, a natural consequence of increased flux of organic acids associated with the shift from tundra vegetation to spruce woodlands throughout the catchments (Whitehead et al., 1989).

The hydrogen-isotope values (δD_{29}) of the basal sample from the Heart Lake record is considerably more positive when compared to its Moose Pond counterpart (Figure 7A and B). While there does appear to be a similar trend to more negative δD_{29} values from older and more positive values at the base of the Moose Pond record, this change is of much smaller magnitude (~15‰). Therefore, we think it unlikely that more positive values in the Heart Lake basal sample are related to a change in regional precipitation patterns within the ADK, or the northeastern United States more broadly. Instead, given that the trend of most positive δD_{29} and δD_{27} is seen at the beginning of record for both basins (Figure 7A and 7B), we suggest that changing catchment vegetation regimes during the period of basin development, as substantiated by the dominance of tundra species in HP Zone 1 at Heart Lake, is the driver of the more positive δD values recorded here for the most basal samples at Heart Lake and Moose Pond.

Several modern-day calibration studies conducted in the Arctic where tundra vegetation is prominent have reported more positive ε_{app} values (the fractionation between source water and leaf wax δD) for some species of modern tundra vegetation compared to the ε_{app} values of temperate forests (Berke et al., 2019; Daniels et al., 2017). For example, Berke et al. (2019) sampled dwarf shrubs, forbs and graminoids for sites in western Greenland and arrived at an average ε_{app} of –86‰ ± 25, where ε_{app} is defined as the fractionation between xylem water and averaged modern plant sample *n*-alkane δD. This is more positive than the similarly calculated

ε_{app} value of –106‰ (σ = 16.0, n = 21), derived from 11 species of modern ADK plant samples (Freimuth et al., 2020). Therefore, the static ε_{app} value best applied to a modern temperate forested environment is likely driving reconstructed precipitation δD to more positive values during the period when the Heart Lake and Moose Pond catchments were composed of greater percentages of non-arboreal forest tundra (Figure 7C and 7D). Using an ε_{app} value of –86‰, for example, would result in a basal δD_{precip} value at Heart Lake of –53.6‰ and at Moose Pond of –93.5‰, considerably more negative than that calculated from an ε_{app} of –123‰ and depicted in Figure 7C.

Furthermore, as the catchments became ice-free, the emerging vegetation assemblages likely contained fewer trees and less canopy than is typical of a temperate forest. An open forest structure of this nature would have a higher potential for evaporative increases in δD and $\delta^{18}O$ values within the soil profile (Shanahan et al., 2013; Faison et al., 2006; Oswald et al., 2018). This mechanism would result in more positive δD *n*-alkane sediment values becoming progressively more negative with time as temperate forest tree species proliferated. This is exactly the trend observed in the basal samples from both Heart Lake and Moose Pond (Figure 7A and 7B).

The physical characteristics of the lake catchments from which sedimentary *n*-alkanes are sourced can have large effects on the distribution of changing vegetation cover through time. Differences in these characteristics may be affecting sedimentary *n*-alkane isotope measurements. In effect, if the more positive values found at the base of Heart Lake and Moose Pond are reflecting catchment specific vegetation composition, then it is no surprise that the excursion maximums seen in the sediment records would be of different magnitude for catchments that differ in size, and elevation. Despite these differences in *n*-alkane δD, overall the appearance of similar chemical profiles for the two lake records suggests that regional processes of lake development were shared in this temperate mountainous environment.

5.3 Holocene Record (~11.5 cal kyr BP – Modern)

At a first order, chemical analysis results from both lakes suggest a stable source of terrestrial organic matter deposition from ~11.5 cal kyr BP through the modern. Throughout both records, C:N values change little and are high (~16), and bulk $\delta^{13}C$ values are also stable (~ –28‰) , as are *n*-C_{29} and *n*-C_{27} $\delta^{13}C$ values (~ –31‰). These data all suggest a dominantly terrestrial carbon source as opposed to aquatic (Figures 5C, 5D, 6C, 6D and A.5 A). Lake productivity likely declined during the late glacial Holocene transition perhaps due to a concomitant decline in weathering rates and nutrient flux into the lake basins. Further, the stability in the chemical records suggests that these lower levels of lake productivity continued through the modern, resulting in the oligotrophic nature of both lakes observed today. Surface sediments at Heart Lake and Moose Pond show TOM values, bulk sediment $\delta^{13}C$, $ACL_{25\text{-}35}$, and compound-specific $\delta^{13}C$ values consistent with results from both lake records beginning ~11.5 cal kyr BP (Freimuth et al., 2020; Figures 5B, 5D, 5F, 6B, 6D, 6F, and A.5). This supports the interpretation of stable and low contributions of aquatic as compared to terrestrial sedimentary organic matter throughout the Holocene.

At a second order, the mixtures of terrestrial sources are different for the two lakes through the Holocene due to catchment size, elevation, and morphology. Both lake records show shifts in *n*-alkane chain-length distributions, but the timing and magnitude of these shifts vary (Figure A.4). At Heart Lake, *n*-C_{29} replaces *n*-C_{27} as the dominant chain length at ~8.5 cal kyr BP and remains at higher concentrations through the modern. This dominance of *n*-C_{27} prior to

~8.5 cal kyr BP is broadly co-incident with HP-Zone 3 (Figure 7D), characterized by a distinct *Pinus* maximum, as well as increasing contributions of *Tsuga* (hemlock) and *Betula,* likely *Betula papyrifera* (paper birch; Whitehead and Jackson, 1990). As *Pinus* and *Tsuga* are gymnosperms, this portion of the *n*-alkane sediment record overlapping with HP-Zone 3 may be biased towards the contribution of the angiosperm *Betula*, as angiosperms have been demonstrated to produce much greater amounts of *n*-alkanes than most gymnosperms (Diefendorf et al., 2015; 2011). Modern species within the genus *Betula* have also been shown to produce greater amounts of *n*-C_{27} relative to *n*-C_{29} (Dawson et al., 2004; Sachse et al., 2006; Schwark et al., 2002; Tarasov et al., 2013; Zech et al., 2010). In modern Adirondack plants for example, *Betula papyrifera* had a C_{27}:C_{29} ratio of ~4.5 (n = 5) while all *Pinus* species had a ratio of ~1.0 (n = 4; Freimuth et al., 2020). Similarly, Sachse et al. (2006) found modern *Betula* samples had maximum chain lengths of 27 at 8 of 10 European sites, compared with overall higher chain-length maximums for other samples (*Quercus*). Pollen zones HP-Zone 4, HP-Zone 5 and HP-Zone 6 also contain high percentages of *Betula (Betula alleghaniensis*; Figure 7D*)*. However, increasing amounts of other high *n*-alkane-producing angiosperm taxa that were established in the catchment in the transition to a mixed conifer-hardwood forest could result in *n*-C_{29} becoming the dominant chain length preserved in the Heart Lake sediment record during the latter part of the Holocene (Figure 5E). In any case, although tying chain-length concentration shifts to a few plant genera is still highly speculative, the similar timing of HP-Zone 3 and dominance of *n*-C_{27} over *n*-C_{29} at Heart Lake is good evidence that local changes in terrestrial vegetation assemblages can be recorded in the leaf wax sediment record for certain sites. In contrast, at Moose Pond, *n*-C_{27} is the dominant chain length through the majority of the record (Figures 6E, and A.4), but concentrations between *n*-C_{29} and *n*-C_{27} show very close tracking from ~8.5 cal kyr BP (Figure A.4 D). Therefore, since we do not see a strong n-C_{29} over n-C_{27} preference at Moose Pond as compared to Heart Lake, the leaf wax compounds were probably contributed to this basin from a different mixture of terrestrial vegetation sources.

This interpretation is consistent with evidence for Early Holocene climate change in the ADK. It is also consistent with the differences in catchment morphology, which would affect the depositional pathways into each lake. Although today both Heart Lake and Moose Pond are situated in the same vegetation zone, in the Early Holocene that may not have been the case. Macrofossil evidence suggests that certain tree taxa moved up the elevational gradient from their modern zonal limits by as much as 300 meters, attributed to higher temperatures and less precipitation during this time period (Jackson, 1989). These changes would exert a stronger influence on a smaller catchment like Heart Lake with less total elevational range (1 km^2, 200 m, Figure 3A) than at Moose Pond (17 km^2, 700 m; Figure 3B). In effect, the terrestrial n-alkane sediment signal would be more biased to a particular vegetation source at Heart Lake, while at Moose Pond the record would be more mixed. Therefore, we would expect a greater degree of sensitivity to vegetation change in the Heart Lake record as opposed to Moose Pond through time. Further, as the coring location at Moose Pond is situated close to a stream inlet, the leaf wax preserved in the sediment record may be from greater distances and of a more diverse source, decreasing the sensitivity to shoreline vegetation assemblages. These mechanisms would allow for variation of terrestrial sources to the sedimentary n-alkane record, even for basins located in the same regional setting.

The n-alkane hydrogen-isotope record from both Heart Lake and Moose Pond show little variability through the Holocene (Figure 7A and 7B). The entire range in δD_{29} and δD_{27} including those of modern surface sediments from the same coring location as this study are only

18.3‰ and 19.4‰ for Heart Lake and 23.3‰ and 20.3‰ for Moose Pond, respectively (Figure 7A and 7B). When comparing the two lake records with each other through time, δD_{29} and δD_{27} values are largely consistent becoming generally more similar the closer to modern day. Comparing between chain lengths at each lake individually, overall δD_{29} and δD_{27} also have very similar values throughout the Holocene (Figure 7A and 7B). A distinct difference between the two *n*-alkane δD records occurs between 11.5 to 8.5 cal kyr BP when the close tracking of δD_{29} and δD_{27} at Moose Pond contrasts with the ~20‰ more positive values of δD_{29} relative to δD_{27} at Heart Lake. As this time frame is roughly equivalent to the HP-Zone 3 of Whitehead and Jackson (1990), this discrepancy between records likely represents variations in the local vegetation assemblage between the two catchments (i.e. the greater influence of *Betula* at Heart Lake) as discussed above. Further evidence that the time period represented by HP-Zone 3 at Heart Lake is influenced by *Betula* is this genera's tendency to show greater hydrogen fractionation in *n*-C_{27} over *n*-C_{29} in the modern (Balascio et al., 2018; Berke et al., 2019; Daniels et al., 2017; Freimuth et al., 2020; Hou, D'Andrea, MacDonald & Huang, 2007; Sachse et al., 2006; Figure A.6), which is consistent with a more positive δD_{29} compared to δD_{27} in the Heart Lake downcore reconstruction (Figure 7B). Given the association with a particular pollen zone and the differences in relative chain-length concentrations, variations in species assemblage between the two lake catchments are therefore likely influencing the δD *n*-alkane values at Heart Lake relative to Moose Pond through the Early Holocene.

5.4 Historic *n*-alkane and reconstructed precipitation δD

The isotopic composition of precipitation is dependent on the source and trajectory of the air parcel, as well as other factors such as temperature of condensation, relative humidity, and rainout (e.g. Dansgaard, 1964). For the northeastern United States, the moisture source exerts a strong control on the resulting hydrogen and oxygen isotope values in precipitation (Burnett et al., 2004; Puntsag et al., 2016; Figure 2). In particular, southern air masses that deliver precipitation to northern New York State in the modern have been demonstrated to be on average ~75‰ enriched in deuterium relative to those from a northern source (Burnett et al., 2004; Figure 2). Modern spring precipitation isotopic content from the Global Network of Isotopes in Precipitation (GNIP) Ottawa station (Figure 1) located in northeastern North America also documents a precipitation δD which varies substantially. From the years 1963 to 2018, the δD value of monthly averaged spring (March to May) precipitation collected at this station ranged 52‰ (IAEA/WMO, 2018). Thus, variations in atmospheric circulation regimes that alter the balance of differently sourced air parcels into the ADK should be recorded in sedimentary *n*-alkane δD.

The Heart Lake and Moose Pond leaf wax records do not provide evidence for large-scale step-changes in spring precipitation sourcing from the end of the late glacial through the Holocene (Figure 7C). In the late glacial samples, the dominant trend at both lakes is from the most positive δD_{precip} values at the base to increasingly more negative values throughout the glacially derived Unit C, but to different degrees (Figure 7C). As discussed in Section 5.2, this pattern likely represents a change in vegetation and canopy structure that obscures the precipitation source signal. The late glacial samples that occur above those sourced from Unit C of each study lake are also consistent with those from the Holocene until ~ 8.5 cal kyr BP, varying only 13.6‰ at Heart Lake and even less (7.3‰) at Moose Pond. Indeed, this variance is similar in magnitude to the average offset seen between the Heart Lake and Moose Pond δD_{precip} values throughout the same interval, which we attribute to vegetation assemblage differences between the two catchments (see Section 5.3). These more positive values observed in the Heart Lake δD_{precip} record may be a permanent feature associated with physical and vegetational differences within the catchments, rather than differences in precipitation isotope values. This is substantiated by modern xylem water and surface sediment data. Heart Lake xylem water δD values from samples collected in May are on average 5.1‰ more positive than their Moose Pond counterparts (Figure 8). Likewise, average surface sediment *n*-alkane δD_{29} measurements from the same coring location as this study are 4.8‰ more positive at Heart Lake compared with Moose Pond. We posit that site-specific characteristics, such as catchment size, slope, aspect and degree of exposure, the relative source of the sedimentary *n*-alkanes within the catchment (shoreline vegetation at Heart Lake as opposed to more distal locations for Moose Pond), and vegetation assemblage differences through time, are contributing to the more positive δD_{precip} observed in the majority of the Heart Lake record.

At ~ 8.5 cal kyr BP, and coincident with the HP Zone 3 and 4 boundary, the δD_{precip} records from both basins tend to converge (Figure 7C and 7D). From 8.5 cal kyr BP to the modern, the δD_{precip} values at Heart Lake are largely within analytical uncertainty of each other, and average –63.3‰ ($\sigma = 4.7$) . The Moose Pond average is similar at –66.0‰ ($\sigma = 6.7$). However, when comparing the Early Holocene (11.5 – 5.5 cal kyr BP) to the Late Holocene (5.5 cal kyr BP – present day), the dD_{precip} values of the former are more positive relative to the later in both records. For example, at Heart Lake the average Early Holocene value is –57.3‰ ($\sigma =$ 4.8), while the Late Holocene average (when including surface sediment data) is –65.0‰ ($\sigma =$ 3.8; Freimuth et al., 2020). Likewise, the Early Holocene average for Moose Pond is –64.0‰ (σ = 5.7), and the Late Holocene average is again more negative at –69.3‰ ($\sigma = 5.5$; Figure 7C). We note that this pattern of more positive isotope values in the Early Holocene and more negative isotope values in the Late Holocene occurs at a similar time interval to that observed in several lake carbonate $\delta^{18}O$ records reported for the northeastern United States and southeastern Canada (e.g. Kirby, Patterson et al., 2002; Kirby, Mullins et al., 2002; Stuiver, 1970; Yu et al., 1997; C. Zhao et al., 2010). However, the average difference in δD_{precip} between the two time periods at each ADK lake is small. The Early Holocene average dD_{precip} value is only 7.6‰ more positive than the Late Holocene average value at Heart Lake, and 5.3‰ more positive at Moose Pond. As the difference in isotope values between these two time periods shows such little variability at both lake sites, we resist interpreting a precipitation source change as a driver of the more negative values in the Late Holocene. In our view, it is equally possible that changes in temperature of precipitation, or minor variations in vegetation assemblage and the associated ε_{app} value, could also produce an average 5 to 10‰ difference in δD_{precip}. Because these time periods also correspond to separate vegetation assemblage zones, at least at Heart Lake, the latter interpretation is not unreasonable (Figure 7C and 7D). The variability in the modern surface sediment data collected in the ADK also cause us to limit our interpretation over such small (10‰) intervals. For example, the δD_{29} values from sediments collected at one cm of depth at 12 ADK lake sites range 21‰ (Freimuth et al., 2020).

The variability in δD_{precip} in the ADK from the end of the late glacial through the Holocene is minimal. It is not consistent with a step change in the dominance of northern versus southern precipitation sourcing to the area, at least at a millennial resolution. Further, this stability in spring atmospheric circulation persisted despite interpreted Holocene changes for this region in effective moisture (e.g. Foster et al., 2006; Marsicek et al., 2013; Menking et al., 2012; Newby et al., 2009; Shuman and Marsicek, 2016; Y. Zhao et al., 2010), sea surface temperatures (Sachs et al., 2007), air temperatures (e.g. Davis et al., 1980; Hou et al., 2012; Oswald et al., 2018; Shuman and Marsicek, 2016) and North Atlantic circulation patterns (Ayache et al., 2018; Hall et al., 2004). Given the stability in the Heart Lake and Moose Pond δD_{precip} downcore record, and the consistency between it and δD_{precip} reconstructed from modern surface sediments, changes in the above climate variables for the northeastern United States are unlikely to be the result of state changes in northern versus southern spring precipitation sourcing trends. It is more likely that the documented changes in Holocene effective moisture and air temperatures for this region were influenced by changes in atmospheric circulation from a different combination of sources, and/or during a season other than spring. The former is suggested by the isotope composition of precipitation from the three primary sources to New York State in the modern. While the southern source has on average a much more positive precipitation δD value (–52‰), the coastal source, which also brings large amounts of precipitation into the region, has an average value of –113‰. This is very similar to the northern continental sourced value of –127‰, and would make resolving the influence of one source from the other difficult in a downcore leaf wax record (Burnett et al., 2004; Figure 2). The later scenario is substantiated by other work from the region which has linked Holocene changes in lake carbonate records with winter atmospheric circulation phenomena, primarily, although not only, the PNA teleconnection pattern (Hubeny et al., 2011; Kirby, Patterson et al., 2002; Kirby, Mullins et al., 2002; Liu et al., 2014; Menking et al., 2012).

The record provided here is one of the only late Quaternary paleoclimate reconstructions for the continental northeastern United States derived from sedimentary terrestrial leaf waxes. Other work in the region has been conducted at coastal sites or has focused on *n*-acids, usually of aquatic as opposed to terrestrial origin (Gao et al., 2017; Hou et al., 2012; Hou, Huang, Oswald, Foster, & Shuman, 2007; Hou et al., 2006; Shuman et al., 2006), making direct comparison of these records to ours difficult. Clearly, more investigations using long-chain terrestrial leaf waxes are needed to understand potential precipitation source changes from the end of the late glacial through the Holocene for northeastern North America. Determining whether the invariant nature of late glacial and Holocene spring precipitation sourcing documented here is the norm or an anomaly can help us understand how synoptic atmospheric circulation patterns might have been integrated into the regional climate system.

6. Conclusions:

(1) The Heart Lake and Moose Pond sediment and carbon-isotope records document lacustrine sedimentation beginning after ~14.0 cal kyr BP. Colonization of the catchments by non-arboreal terrestrial vegetation followed shortly after, before the vegetation assemblage transitioned rapidly into that of a temperate forested environment. Initial levels of lake productivity dropped significantly in the earliest Holocene, concomitant with increases in sedimentary organic matter from vascular plants, which became the dominate carbon source through to modern day.

(2) The Heart Lake *n*-alkane δD_{29} and δD_{27} values are overall slightly more positive relative to their Moose Pond counterparts throughout the majority of record. Through the Early Holocene, δD_{27} is distinctly more negative relative to δD_{29} at Heart Lake compared to Moose Pond. These differences, and those in *n*-alkane concentration ratios between the two sites, are likely due to variations in lake catchment size, morphology, elevation and vegetation assemblage.

(3) Reconstructed δD_{precip} values from Heart Lake and Moose Pond are largely invariant through the time of record, and range only ~22‰ through the Holocene. Therefore, the

sedimentary δD leaf wax record provides no evidence for high magnitude synoptic spring atmospheric circulation changes from the end of the late glacial through the Holocene in the Adirondacks.

Acknowledgements:

We would like to thank Dr. Catherine Yansa for her help in identifying several macrofossils for radiocarbon analysis, Andrew Diefendorf for constructing the core refrigeration unit, and Helen Eifert and Elliot Boyd for field assistance. We also thank Jonathan DeSantis and Barbara Lucas-Wilson of the New York State Department of Environmental Conservation for their assistance with sampling permits, and the Adirondack Mountain Club for granting access to Heart Lake. Invaluable assistance was also provided by two anonymous reviewers and Dr. Susan Zimmerman whose critiques and suggestions led to a much-refined version of this manuscript. This research was supported by the US National Science Foundation grants EAR-1229114 to AFD, EAR-1636740 (to AFD and TVL), EAR-1636744 to AK Stewart and EAR-1602789 to TVL.

Appendix A. Supplementary data:

The supplementary data and information to this article can be accessed online at .

References:

Amini, S., & Straus, D. M. (2019). Control of Storminess over the Pacific and North America by Circulation Regimes. *Climate Dynamics, 52*(7), 4749-4770. doi:10.1007/s00382-018-4409-7

Appleby, P.G., & Oldfield, F. (1978). The calculation of ^{210}Pb dates assuming a constant rate of supply of unsupported ^{210}Pb to the sediment. *Catena 5*, 1-8.

April, R. H., Keller, D., & Driscoll, C. T. (2004). Smectite in spodosols from the Adirondack Mountains of New York. *Clay Minerals, 39*(1), 99-113. doi:10.1180/0009855043910123

April, R. H., & Newton, R. M. (1983). Mineralogy and chemistry of some Adirondack spodosols. *Soil Science, 135*(5), 301-307.

Arguez, A., Durre, I., Applequist, S., Squires, M., Vose, R., Yin, X., & Bilotta , R. (2010). NOAA's U.S. Climate Normals (1981-2010). [USC00304555; USC00305714; USC00306957; USW00094740; USC00302554; USC00308631]. NOAA National Centers for Environmental Information. DOI:10.7289/V5PN93JP [June 1, 2019].

Arseneau, K. M. A., Driscoll, C. T., Cummings, C. M., Pope, G., & Cumming, B. F. (2016). Adirondack (NY, USA) reference lakes show a pronounced shift in chrysophyte species composition since ca. 1900. *Journal of Paleolimnology, 56*(4), 349-364. doi:10.1007/s10933-016-9922-2

Arseneau, K. M. A., Driscoll, C. T., Brager, L. M., Ross, K. A., & Cumming, B. F. (2011). Recent evidence of biological recovery from acidification in the Adirondacks (New York, USA): a multiproxy paleolimnological investigation of Big Moose Lake. *Canadian Journal of Fisheries and Aquatic Sciences, 68*(4), 575-592. doi:10.1139/f2011-003

Ayache, M., Swingedouw, D., Mary, Y., Eynaud, F., & Colin, C. (2018). Multi-centennial variability of the AMOC over the Holocene: A new reconstruction based on multiple proxy-derived SST records. *Global and Planetary Change, 170*, 172-189. doi:https://doi.org/10.1016/j.gloplacha.2018.08.016

Balascio, N. L., D'Andrea, W. J., Anderson, R. S., & Wickler, S. (2018). Influence of vegetation type on n-alkane composition and hydrogen isotope values from a high latitude ombrotrophic bog. *Organic Geochemistry, 121*, 48-57. doi:https://doi.org/10.1016/j.orggeochem.2018.03.008

Ballantyne, C. K. (2002). Paraglacial geomorphology. *Quaternary Science Reviews, 21*(18), 1935-2017. doi:https://doi.org/10.1016/S0277-3791(02)00005-7

Barth, A. M., Marcott, S. A., Licciardi, J. M., & Shakun, J. D. (2019). Deglacial Thinning of the Laurentide Ice Sheet in the Adirondack Mountains, New York, USA, Revealed by ^{36}Cl Exposure Dating. *Paleoceanography and Paleoclimatology*. doi:10.1029/2018pa003477

Beria, H., Larsen, J. R., Ceperley, N. C., Michelon, A., Vennemann, T., & Schaefli, B. (2018). Understanding snow hydrological processes through the lens of stable water isotopes. *Wiley Interdisciplinary Reviews: Water, 5*(6) e1311. doi:10.1002/wat2.1311

Berke, M. A., Cartagena Sierra, A., Bush, R., Cheah, D., & O'Connor, K. (2019). Controls on leaf wax fractionation and δ2H values in tundra vascular plants from western Greenland. *Geochimica et Cosmochimica Acta, 244*, 565-583. doi:https://doi.org/10.1016/j.gca.2018.10.020

Bhattacharya, T., Tierney, J. E., Addison, J. A., & Murray, J. W. (2018). Ice-sheet modulation of deglacial North American monsoon intensification. *Nature Geoscience, 11*(11), 848-852. doi:10.1038/s41561-018-0220-7

Bird, B. W., Polisar, P. J., Lei, Y., Thompson, L. G., Yao, T., Finney, B. P., Bain, D. J., Pompeani, D. P. & Steinman, B. A. (2014). A Tibetan lake sediment record of Holocene Indian summer monsoon variability. *Earth and Planetary Science Letters, 399*, 92-102. doi:https://doi.org/10.1016/j.epsl.2014.05.017

Binford, M. W. (1990). Calculation and uncertainty analysis of 210Pb dates for PIRLA project lake sediment cores. *Journal of Paleolimnology, 3*(3), 253-267. doi:10.1007/BF00219461

Blaauw, M., & Christen, J. A. (2011). Flexible paleoclimate age-depth models using an autoregressive gamma process. *Bayesian Anal., 6*(3), 457-474. doi:10.1214/11-BA618

Bowen G.J. (2018). The Online Isotopes in Precipitation Calculator, version 3.1. http://www.waterisotopes.org.

Bowen, G. J., & Revenaugh, J. (2003). Interpolating the isotopic composition of modern meteoric precipitation. *Water Resources Research, 39*(10), 1299. doi:10.1029/2003wr002086

Bradbury, J. A., Dingman, S. L., & Keim, B. D. (2002). New England drought and relations with large scale atmospheric circulation patterns. *Journal of the American Water Resources Association, 38*(5), 1287-1299. doi:10.1111/j.1752-1688.2002.tb04348.x

Bryson, R.A. & Hare, F.K. (Eds.). (1974). Climates of North America. In *World Survey of Climatology* (Vol. 11). Amsterdam, NY: Elsevier Publishing Co..

Burnett, A. W., Mullins, H. T., & Patterson, W. P. (2004). Relationship between atmospheric circulation and winter precipitation δ18O in central New York State. *Geophysical Research Letters, 31*(22), L22209. doi:10.1029/2004gl021089

Chang Huang, C., MacDonald, G., & Cwynar, L. (2004). Holocene landscape development and climatic change in the low arctic, Northwest Territories, Canada. *Palaeogeography, Palaeoclimatology, Palaeoecology, 205*(3), 221-234. doi:https://doi.org/10.1016/j.palaeo.2003.12.009

Church, M., & Ryder, J. M. (1972). Paraglacial Sedimentation: A Consideration of Fluvial Processes Conditioned by Glaciation. *GSA Bulletin, 83*(10), 3059-3072. doi:10.1130/0016-7606(1972)83[3059:psacof]2.0.co;2

Coplen, T. B., Brand, W. A., Gehre, M., Gröning, M., Meijer, H. A. J., Toman, B., & Verkouteren, R. M. (2006). New Guidelines for δ13C Measurements. *Analytical Chemistry, 78*(7), 2439-2441. doi:10.1021/ac052027c

Craft, J. L. (1979). Evidence of local glaciation, Adirondack Mountains, N.Y.. 42nd Annual Reunion, Eastern Friends of the Pleistocene, 75 pp.

Crann, C. A., Patterson, R. T., Macumber, A. L., Galloway, J. M., Roe, H. M., Blaauw, M., Swindles, G. T. & Falck, H. (2015). Sediment accumulation rates in subarctic lakes: Insights into age-depth modeling from 22 dated lake records from the Northwest Territories, Canada. *Quaternary Geochronology, 27*, 131-144. doi:https://doi.org/10.1016/j.quageo.2015.02.001

Cwynar, L. C., & Spear, R. W. (2001). Late glacial climate change in the White Mountains of New Hampshire. *Quaternary Science Reviews, 20*(11), 1265-1274. doi:https://doi.org/10.1016/S0277-3791(00)00151-7

Daniels, W. C., Russell, J. M., Giblin, A. E., Welker, J. M., Klein, E. S., & Huang, Y. (2017). Hydrogen isotope fractionation in leaf waxes in the Alaskan Arctic tundra. *Geochimica et Cosmochimica Acta, 213*, 216-236. doi:https://doi.org/10.1016/j.gca.2017.06.028

Dansgaard, W. (1964). Stable isotopes in precipitation. *Tellus, 16*(4), 436-468. doi:10.1111/j.2153-3490.1964.tb00181.x

Davis, M. B., Spear, R. W., & Shane, L. C. K. (1980). Holocene climate of New England. *Quaternary Research, 14*(2), 240-250. doi:https://doi.org/10.1016/0033-5894(80)90051-4

Dawson, L. A., Towers, W., Mayes, R. W., Craig, J., Väisänen, R. K., & Waterhouse, E. C. (2004). The use of plant hydrocarbon signatures in characterizing soil organic matter. *Geological Society, London, Special Publications, 232*(1), 269-276. doi:10.1144/gsl.sp.2004.232.01.24

Diefendorf, A. F., Patterson, W. P., Holmden, C., & Mullins, H. T. (2008). Carbon isotopes of marl and lake sediment organic matter reflect terrestrial landscape change during the late Glacial and early Holocene (16,800 to 5,540 cal yr B.P.): a multiproxy study of lacustrine sediments at Lough Inchiquin, western Ireland. *Journal of Paleolimnology, 39*(1), 101-115. doi:10.1007/s10933-007-9099-9

Diefendorf, A. F., & Freimuth, E. J. (2017). Extracting the most from terrestrial plant-derived n-alkyl lipids and their carbon isotopes from the sedimentary record: A review. *Organic Geochemistry, 103*, 1-21. doi:https://doi.org/10.1016/j.orggeochem.2016.10.016

Diefendorf, A. F., Leslie, A. B., & Wing, S. L. (2015). Leaf wax composition and carbon isotopes vary among major conifer groups. *Geochimica et Cosmochimica Acta, 170*, 145-156. doi:https://doi.org/10.1016/j.gca.2015.08.018

Diefendorf, A. F., Freeman, K. H., Wing, S. L., & Graham, H. V. (2011). Production of n-alkyl lipids in living plants and implications for the geologic past. *Geochimica et Cosmochimica Acta, 75*(23), 7472-7485. doi:https://doi.org/10.1016/j.gca.2011.09.028

Driscoll, C. T., Driscoll, K. M., Fakhraei, H., & Civerolo, K. (2016). Long-term temporal trends and spatial patterns in the acid-base chemistry of lakes in the Adirondack region of New York in response to decreases in acidic deposition. *Atmospheric Environment, 146*, 5-14. doi:https://doi.org/10.1016/j.atmosenv.2016.08.034

Driscoll, C. T., & Newton, R. M. (1985). Chemical characteristics of Adirondack lakes. *Environmental Science & Technology, 19*(11), 1018-1024. doi:10.1021/es00141a604

Driscoll C.T., Newton R.M., Gubala C.P., Baker J.P. and Christensen S.W. (1991). Adirondack Mountains. In D.F. Charles and S. Christie (Eds.), *Acidic deposition and aquatic ecosystems* (pp. 133-202). New York: Springer-Verlag.

Eglinton, G., & Hamilton, R. J. (1967). Leaf Epicuticular Waxes. *Science, 156*(3780), 1322-1335. doi:10.1126/science.156.3780.1322

Faison, E. K., Foster, D. R., Oswald, W. W., Hansen, B. C. S., & Doughty, E. (2006). Early Holocene openlands in southern New England. *Ecology, 87*(10), 2537-2547. doi:10.1890/0012-9658(2006)87[2537:ehoisn]2.0.co;2

Feakins, S. J., Wu, M. S., Ponton, C., & Tierney, J. E. (2019). Biomarkers reveal abrupt switches in hydroclimate during the last glacial in southern California. *Earth and Planetary Science Letters, 515*, 164-172. doi:https://doi.org/10.1016/j.epsl.2019.03.024

Ficken, K. J., Li, B., Swain, D. L., & Eglinton, G. (2000). An n-alkane proxy for the sedimentary input of submerged/floating freshwater aquatic macrophytes. *Organic Geochemistry, 31*(7), 745-749. doi:https://doi.org/10.1016/S0146-6380(00)00081-4

Foster, D. R., Oswald, W. W., Faison, E. K., Doughty, E. D., & Hansen, B. C. S. (2006). A Climate driver for abrupt Mid-Holocene vegetation dynamics and the Hemlock decline in New England. *Ecology, 87*(12), 2959-2966. doi:10.1890/0012-9658(2006)87[2959:acdfam]2.0.co;2

Freimuth, E.J., Diefendorf, A.F., Lowell, T.V., Bates, B.R., Schartman, A.K., Bird, B.W., Landis, J.D., & Stewart, A.K. (2020). Contrasting sensitivity of lake sediment *n*-alkane and *n*-alkanoic acids to basin-scale vegetation and regional-scale precipitation δ^2H in the Adirondack Mountains, NY (USA). *Geochimica et Cosmochimica Acta*. doi: https://doi.org/10.1016/j.gca.2019.08.026.

Freimuth, E. J., Diefendorf, A. F., Lowell, T. V., & Wiles, G. C. (2019). Sedimentary *n*-alkanes and *n*-alkanoic acids in a temperate bog are biased toward woody plants. *Organic Geochemistry, 128*, 94-107. doi:https://doi.org/10.1016/j.orggeochem.2019.01.006

Freimuth, E. J., Diefendorf, A. F., & Lowell, T. V. (2017). Hydrogen isotopes of n-alkanes and n-alkanoic acids as tracers of precipitation in a temperate forest and implications for paleorecords. *Geochimica et Cosmochimica Acta, 206*, 166-183. doi:https://doi.org/10.1016/j.gca.2017.02.027

Fritz, S.C., & Anderson, N.J. (2013). The relative influences of climate and catchment processes on Holocene lake development in glaciated regions. *Journal of Paleolimnology*, *49*, 349- 362. doi:https://doi.org/10.1007/s10933-013-9684-z

Fukushima, A., Kanamori, H., & Matsumoto, J. (2019). Regionality of long-term trends and interannual variation of seasonal precipitation over India. *Progress in Earth and Planetary Science, 6*(1), 1-20. doi:10.1186/s40645-019-0255-4

Gao, L., Huang, Y., Shuman, B., Oswald, W. W., & Foster, D. (2017). A high-resolution hydrogen isotope record of behenic acid for the past 16 kyr in the northeastern United States. *Quaternary International, 449*, 1-11. doi:https://doi.org/10.1016/j.quaint.2017.06.053

Garcin, Y., Schefuß, E., Schwab, V. F., Garreta, V., Gleixner G., Vincens, A., Todou, G., Séné, O., Onana, J.-M., Achoundong, G. & Sachse, D. (2014). Reconstructing C3 and C4 vegetation cover using n-alkane carbon isotope ratios in recent lake sediments from Cameroon, Western Central Africa. *Geochimica et Cosmochimica Acta, 142*, 482-500. doi:https://doi.org/10.1016/j.gca.2014.07.004

Gray, A. B., Pasternack, G. B., & Watson, E. B. (2010). Hydrogen peroxide treatment effects on the particle size distribution of alluvial and marsh sediments. *The Holocene, 20*(2), 293-301. doi:10.1177/0959683609350390

Hall, I. R., Bianchi, G. G., & Evans, J. R. (2004). Centennial to millennial scale Holocene climate-deep water linkage in the North Atlantic. *Quaternary Science Reviews, 23*(14), 1529-1536. doi:https://doi.org/10.1016/j.quascirev.2004.04.004

Hartley, S., & Keables, M. J. (1998). Synoptic associations of winter climate and snowfall variability in New England, USA, 1950–1992. *International Journal of Climatology, 18*(3), 281-298. doi:10.1002/(sici)1097-0088(19980315)18:3<281::aid-joc245>3.0.co;2-f

Heiri, O., Lotter, A. F., & Lemcke, G. (2001). Loss on ignition as a method for estimating organic and carbonate content in sediments: reproducibility and comparability of results. *Journal of Paleolimnology, 25*(1), 101-110. doi:10.1023/a:1008119611481

Henderson, A. K., & Shuman, B. N. (2009). Hydrogen and oxygen isotopic compositions of lake water in the western United States. *GSA Bulletin, 121*(7-8), 1179-1189. doi:10.1130/b26441.1

Hou, J., Huang, Y., Shuman, B. N., Oswald, W. W., & Foster, D. R. (2012). Abrupt cooling repeatedly punctuated early-Holocene climate in eastern North America. *The Holocene, 22*(5), 525-529. doi:10.1177/0959683611427329

Hou, J., D'Andrea, W. J., MacDonald, D., & Huang, Y. (2007). Hydrogen isotopic variability in leaf waxes among terrestrial and aquatic plants around Blood Pond, Massachusetts (USA). *Organic Geochemistry, 38*(6), 977-984. doi:https://doi.org/10.1016/j.orggeochem.2006.12.009

Hou, J., Huang, Y., Oswald, W. W., Foster, D. R., & Shuman, B. (2007). Centennial-scale compound-specific hydrogen isotope record of Pleistocene–Holocene climate transition from southern New England, *Geophysical Research Letters*, *34*(19). doi:10.1029/2007GL30303.

Hou, J., Huang, Y., Wang, Y., Shuman, B., Oswald, W. W., Faison, E., & Foster, D. R. (2006). Postglacial climate reconstruction based on compound-specific D/H ratios of fatty acids from Blood Pond, New England. *Geochemistry, Geophysics, Geosystems, 7*(3), Q03008. doi:10.1029/2005gc001076

Hubeny, J. B., King, J. W., & Reddin, M. (2011). Northeast US precipitation variability and North American climate teleconnections interpreted from late Holocene varved sediments. *Proceedings of the National Academy of Sciences, 108*(44), 17895-17900. doi:10.1073/pnas.1019301108

IAEA/WMO (2018). Global Network of Isotopes in Precipitation. The GNIP Database. Accessible at: https://nucleus.iaea.org/wiser.

Isachsen, Y.W., & Fisher, D.W. (1970) Geologic map of New York, Adirondack sheet: New York State Museum and Science Service Map and Chart Series 15.

Ito, M., Mitchell, M. J., & Driscoll, C. T. (2002). Spatial patterns of precipitation quantity and chemistry and air temperature in the Adirondack region of New York. *Atmospheric Environment, 36*(6), 1051-1062. doi:https://doi.org/10.1016/S1352-2310(01)00484-8

Jackson, S. T. (1989). Postglacial vegetational changes along an elevational gradient in the Adirondack Mountains (New York): a study of plant macrofossils. Albany, NY: University of the State of New York, State Education Dept., New York State Museum, Biological Survey.

Jackson, S. T. (1990). Pollen source area and representation in small lakes of the northeastern United States. *Review of Palaeobotany and Palynology, 63*(1), 53-76. doi:https://doi.org/10.1016/0034-6667(90)90006-5

Jackson, S. T., & Whitehead, D. R. (1991). Holocene Vegetation Patterns in the Adirondack Mountains. *Ecology, 72*(2), 641-653. doi:10.2307/2937204

Kahmen, A., Dawson, T. E., Vieth, A., & Sasche, D. (2011). Leaf wax n-alkane δD values are determined early in the ontogeny of Populus trichocarpa leaves when grown under controlled environmental conditions. *Plant, Cell & Environment, 34*(10), 1639-1651. doi:10.1111/j.1365-3040.2011.02360.x

Kirby, M., Patterson, W., Mullins, H., & Burnett, A. (2002). Post-Younger Dryas climate interval linked to circumpolar vortex variability: isotopic evidence from Fayetteville Green Lake, New York. *Climate Dynamics, 19*(3), 321-330. doi:10.1007/s00382-002-0227-y

Kirby, M. E., Mullins, H. T., Patterson, W. P., & Burnett, A. W. (2002). Late glacial–Holocene atmospheric circulation and precipitation in the northeast United States inferred from modern calibrated stable oxygen and carbon isotopes. *GSA Bulletin, 114*(10), 1326-1340. doi:10.1130/0016-7606(2002)114<1326:lghaca>2.0.co;2

Landis, J. D., Renshaw, C. E., & Kaste, J. M. (2012). Measurement of 7Be in soils and sediments by gamma spectroscopy. *Chemical Geology, 291*, 175-185. doi:https://doi.org/10.1016/j.chemgeo.2011.10.007

Lavoie, M., Pellerin, S., Larocque, M., & Bottollier-Curtet, M. (2015). Late glacial and Holocene vegetation history in the northern foothills of the Adirondack mountains. *Écoscience, 22*(1), 59-70. doi:http://dx.doi.org.proxy.libraries.uc.edu/10.1080/11956860.2015.1052203

Liu, Z., Yoshimura, K., Bowen, G. J., Buenning, N. H., Risi, C., Welker, J. M., & Yuan, F. (2014). Paired oxygen isotope records reveal modern North American atmospheric dynamics during the Holocene. *Nature Communications, 5*, 3701. doi:http://dx.doi.org.proxy.libraries.uc.edu/10.1038/ncomms4701

Marsicek, J. P., Shuman, B., Brewer, S., Foster, D. R., & Oswald, W. W. (2013). Moisture and temperature changes associated with the mid-Holocene Tsuga decline in the northeastern United States. *Quaternary Science Reviews, 80*, 129-142. doi:https://doi.org/10.1016/j.quascirev.2013.09.001

Marzi, R., Torkelson, B. E., & Olson, R. K. (1993). A revised carbon preference index. *Organic Geochemistry, 20*(8), 1303-1306. doi:https://doi.org/10.1016/0146-6380(93)90016-5

McFadden, M. A., Patterson, W. P., Mullins, H. T., & Anderson, W. T. (2005). Multi-proxy approach to long- and short-term Holocene climate-change: evidence from eastern Lake Ontario. *Journal of Paleolimnology, 33*(3), 371-391. doi:10.1007/s10933-004-7634-5

Menking, K. M., Peteet, D. M., & Anderson, R. Y. (2012). Late-glacial and Holocene vegetation and climate variability, including major droughts, in the Sky Lakes region of southeastern New York State. *Palaeogeography, Palaeoclimatology, Palaeoecology, 353-355*, 45-59. doi:https://doi.org/10.1016/j.palaeo.2012.06.033

Meyers, P. A., & Lallier-vergés, E. (1999). Lacustrine Sedimentary Organic Matter Records of Late Quaternary Paleoclimates. *Journal of Paleolimnology, 21*(3), 345-372. doi:10.1023/a:1008073732192

Meyers, P. A. (2003). Applications of organic geochemistry to paleolimnological reconstructions: a summary of examples from the Laurentian Great Lakes. *Organic Geochemistry, 34*(2), 261-289. doi:https://doi.org/10.1016/S0146-6380(02)00168-7

Miller, E. K., Friedland, A. J., Arons, E. A., Mohnen, V. A., Battles, J. J., Panek, J. A., Kadlecek, J. & Johnson, A. H. (1993). Atmospheric deposition to forests along an elevational gradient at Whiteface Mountain, NY, U.S.A. *Atmospheric Environment. Part A. General Topics, 27*(14), 2121-2136. doi:https://doi.org/10.1016/0960-1686(93)90042-W

Mullon, L., Chang, N.-B., Jeffrey Yang, Y., & Weiss, J. (2013). Integrated remote sensing and wavelet analyses for screening short-term teleconnection patterns in northeast America. *Journal of Hydrology, 499*, 247-264. doi:https://doi.org/10.1016/j.jhydrol.2013.06.046

Newby, P. E., Donnelly, J. P., Shuman, B. N., & MacDonald, D. (2009). Evidence of centennial-scale drought from southeastern Massachusetts during the Pleistocene/Holocene transition. *Quaternary Science Reviews, 28*(17), 1675-1692. doi:https://doi.org/10.1016/j.quascirev.2009.02.020

Olson, D. M., Dinerstein, E., Wikramanayake, E. D., Burgess, N. D., Powell, G. V. N., Underwood, E. C., D'amico, J. A., Itoua, I., Strand, H. E., Morrison, J. C., Loucks, C. J., Allnutt, T. F., Ricketts, T. H., Kura, Y., Lamoreux, J. F., Wettengel, W. W., Hedao, P. and Kassem, K. R. (2001). Terrestrial Ecoregions of the World: A New Map of Life on Earth. *BioScience, 51*(11), 933-938.

Oswald, W. W., Foster, D. R., Shuman, B. N., Doughty, E. D., Faison, E. K., Hall, B. R., Hansen, B. C. S., Lindbladh, M., Marroquin, A. & Truebe, S. A. (2018). Subregional variability in the response of New England vegetation to postglacial climate change. *45*(10), 2375-2388. doi:10.1111/jbi.13407

Overpeck, J. T. (1985). A pollen study of a late Quaternary peat bog, south-central Adirondack Mountains, New York. *GSA Bulletin, 96*(1), 145-154. doi:10.1130/0016-7606(1985)96<145:apsoal>2.0.co;2

Peel, M. C., Finlayson, B. L., & McMahon, T. A. (2007). Updated world map of the Köppen-Geiger climate classification. *Hydrol. Earth Syst. Sci., 11*(5), 1633-1644. doi:10.5194/hess-11-1633-2007

Polissar, P. J., & D'Andrea, W. J. (2014). Uncertainty in paleohydrologic reconstructions from molecular δD values. *Geochimica et Cosmochimica Acta, 129*, 146-156. doi:https://doi.org/10.1016/j.gca.2013.12.021

Polissar, P. J., & Freeman, K. H. (2010). Effects of aridity and vegetation on plant-wax δD in modern lake sediments. *Geochimica et Cosmochimica Acta, 74*(20), 5785-5797. doi:https://doi.org/10.1016/j.gca.2010.06.018

Puntsag, T., Mitchell, M. J., Campbell, J. L., Klein, E. S., Likens, G. E., & Welker, J. M. (2016). Arctic Vortex changes alter the sources and isotopic values of precipitation in northeastern US. *Scientific Reports, 6*, 22647. doi:10.1038/srep22647

Rach, O., Brauer, A., Wilkes, H., & Sachse, D. (2014). Delayed hydrological response to Greenland cooling at the onset of the Younger Dryas in western Europe. *Nature Geoscience, 7*, 109. doi:10.1038/ngeo2053

Reimer, P., Bard, E., Bayliss, A., Beck, J., Blackwell, P., Bronk Ramsey, C., Buck, C., Cheng, H., Edwards, R., Friedrich, M., Grootes, P., Guilderson, T., Haflidason, H., Hajdas, I., Hatté, C., Heaton, T., Hoffmann, D., Hogg, A., Hughen, K., Kaiser, K., Kromer, B., Manning, S., Niu, M., Reimer, R., Richards, D., Scott, E., Southon, J., Staff, R., Turney, C., & van der Plicht, J. (2013). IntCal13 and Marine13 Radiocarbon Age Calibration Curves 0–50,000 Years cal BP. *Radiocarbon, 55*(4), 1869-1887.

Sachs, J. P. (2007). Cooling of Northwest Atlantic slope waters during the Holocene. *Geophysical Research Letters, 34*(3). doi:10.1029/2006gl028495

Sachse, D., Billault, I., Bowen, G. J., Chikaraishi, Y., Dawson, T. E., Feakins, S. J., Freeman, K. H., Magill, C. R., McInerney, F. A., Meer, M. T. J. v. d., Polissar, P., Robins, R. J., Sachs, J. P., Schmidt, H.-L., Sessions, A. L., White, J. W. C., West, J. B. & Kahmen, A. (2012). Molecular Paleohydrology: Interpreting the Hydrogen-Isotopic Composition of Lipid Biomarkers from Photosynthesizing Organisms. *Annual Review of Earth and Planetary Sciences, 40*(1), 221-249. doi:10.1146/annurev-earth-042711-105535

Sachse, D., Gleixner, G., Wilkes, H., & Kahmen, A. (2010). Leaf wax n-alkane δD values of field-grown barley reflect leaf water δD values at the time of leaf formation. *Geochimica et Cosmochimica Acta, 74*(23), 6741-6750. doi:https://doi.org/10.1016/j.gca.2010.08.033

Sachse, D., Radke, J., & Gleixner, G. (2006). δD values of individual n-alkanes from terrestrial plants along a climatic gradient – Implications for the sedimentary biomarker record. *Organic Geochemistry, 37*(4), 469-483. doi:https://doi.org/10.1016/j.orggeochem.2005.12.003

Sachse, D., Radke, J., & Gleixner, G. (2004). Hydrogen isotope ratios of recent lacustrine sedimentary n-alkanes record modern climate variability. *Geochimica et Cosmochimica Acta, 68*(23), 4877-4889. doi:https://doi.org/10.1016/j.gca.2004.06.004

Schlesinger, W., & Reiners, W. (1974). Deposition of Water and Cations on Artificial Foliar Collectors in Fir Krummholz of New England Mountains. *Ecology, 55*(2), 378-386. doi:10.2307/1935225

Schwark, L., Zink, K., & Lechterbeck, J. (2002). Reconstruction of postglacial to early Holocene vegetation history in terrestrial Central Europe via cuticular lipid biomarkers and pollen records from lake sediments. *Geology, 30*(5), 463-466. doi:10.1130/0091-7613(2002)030<0463:ropteh>2.0.co;2

Schwartz, M. W. (1989). Predicting tree frequencies from pollen frequency: an attempt to validate the R value method. *New Phytologist, 112*(1), 129-143. doi:10.1111/j.1469-8137.1989.tb00318.x

Seki, O., Nakatsuka, T., Shibata, H., & Kawamura, K. (2010). A compound-specific n-alkane δ13C and δD approach for assessing source and delivery processes of terrestrial organic matter within a forested watershed in northern Japan. *Geochimica et Cosmochimica Acta, 74*(2), 599-613. doi:https://doi.org/10.1016/j.gca.2009.10.025

Shanahan, T. M., Hughen, K. A., Ampel, L., Sauer, P. E., & Fornace, K. (2013). Environmental controls on the 2H/1H values of terrestrial leaf waxes in the eastern Canadian Arctic. *Geochimica et Cosmochimica Acta, 119*, 286-301. doi:https://doi.org/10.1016/j.gca.2013.05.032

Shuman, B. N., & Marsicek, J. (2016). The structure of Holocene climate change in mid-latitude North America. *Quaternary Science Reviews, 141*, 38-51. doi:https://doi.org/10.1016/j.quascirev.2016.03.009

Shuman, B., Huang, Y., Newby, P., & Wang, Y. (2006). Compound-specific isotopic analyses track changes in seasonal precipitation regimes in the Northeastern United States at ca 8200calyrBP. *Quaternary Science Reviews, 25*(21), 2992-3002. doi:https://doi.org/10.1016/j.quascirev.2006.02.021

Shuman, B. (2003). Controls on loss-on-ignition variation in cores from two shallow lakes in the northeastern United States. *Journal of Paleolimnology, 30*(4), 371-385. doi:10.1023/B:JOPL.0000007226.68831.e3

Stein, A. F., Draxler, R. R., Rolph, G. D., Stunder, B. J. B., Cohen, M. D., & Ngan, F. (2015). NOAA's HYSPLIT Atmospheric Transport and Dispersion Modeling System. *Bulletin of the American Meteorological Society, 96*(12), 2059-2077. doi:10.1175/bams-d-14-00110.1

Stuiver, M. (1970). Oxygen and carbon isotope ratios of fresh-water carbonates as climatic indicators. *Journal of Geophysical Research, 75*(27), 5247-5257. doi:10.1029/JC075i027p05247

Sullivan, T. J., Fernandez, I. J., Herlihy, A. T., Driscoll, C. T., McDonnell, T. C., Nowicki, N. A., Snyder, K. U. & Sutherland, J. W. (2006). Acid-base Characteristics of Soils in the Adirondack Mountains, New York. *Soil Science Society of America Journal, 70*(1), 141-152. doi:10.2136/sssaj2005.0073

Tarasov, P. E., Müller, S., Zech, M., Andreeva, D., Diekmann, B., & Leipe, C. (2013). Last glacial vegetation reconstructions in the extreme-continental eastern Asia: Potentials of pollen and n-alkane biomarker analyses. *Quaternary International, 290-291*, 253-263. doi:https://doi.org/10.1016/j.quaint.2012.04.007

Thomas, E. K., Huang, Y., Clemens, S. C., Colman, S. M., Morrill, C., Wegener, P., & Zhao, J. (2016). Changes in dominant moisture sources and the consequences for hydroclimate on the northeastern Tibetan Plateau during the past 32 kyr. *Quaternary Science Reviews, 131*, 157-167. doi:https://doi.org/10.1016/j.quascirev.2015.11.003

Tierney, J. E., Oppo, D. W., Rosenthal, Y., Russell, J. M., & Linsley, B. K. (2010). Coordinated hydrological regimes in the Indo-Pacific region during the past two millennia. *Paleoceanography, 25*(1), PA1102. doi:10.1029/2009pa001871

Tipple, B. J., Berke, M. A., Doman, C. E., Khachaturyan, S., & Ehleringer, J. R. (2013). Leaf-wax n-alkanes record the plant–water environment at leaf flush. *Proceedings of the National Academy of Sciences, 110*(7), 2659-2664. doi:10.1073/pnas.1213875110

Veals, P. G., & Steenburgh, W. J. (2015). Climatological Characteristics and Orographic Enhancement of Lake-Effect Precipitation East of Lake Ontario and over the Tug Hill Plateau. *Monthly Weather Review, 143*(9), 3591-3609. doi:10.1175/mwr-d-15-0009.1

Webb, T., Howe, S. E., Bradshaw, R. H. W., & Heide, K. M. (1981). Estimating plant abundances from pollen percentages: The use of regression analysis. *Review of Palaeobotany and Palynology, 34*(3), 269-300. doi:https://doi.org/10.1016/0034-6667(81)90046-4

Whitehead, D. R., & Jackson, S. T. (1990). The regional vegetational history of the High Peaks (Adirondack Mountains) New York. Albany, NY: University of the State of New York, State Education Dept., New York State Museum, Biological Survey.

Whitehead, D. R., Charles, D. F., Jackson, S. T., Smol, J. P., & Engstrom, D. R. (1989). The developmental history of Adirondack (N.Y.) lakes. *Journal of Paleolimnology, 2*(3), 185-206. doi:10.1007/bf00202046

Xu, K., Lu, R., Kim, B.J., Park, J.K., Mao, J., Byon, J.Y., Chen, R. and Kim, E.B. (2019). Large-Scale Circulation Anomalies Associated with Extreme Heat in South Korea and Southern–Central Japan. *Journal of Climate, 32*(10), 2747-2759. doi:10.1175/jcli-d-18-0485.1

Yu, Z. (2000). Ecosystem response to Lateglacial and early Holocene climate oscillations in the Great Lakes region of North America, *Quaternary Science Reviews,* 19(17), 1723-1747.

Yu, Z., McAndrews, J. H., & Eicher, U. (1997). Middle Holocene dry climate caused by change in atmospheric circulation patterns: Evidence from lake levels and stable isotopes. *Geology, 25*(3), 251-254. doi:10.1130/0091-7613(1997)025<0251:mhdccb>2.3.co;2

Zarfos, M. R., Dovciak, M., Lawrence, G. B., McDonnell, T. C., & Sullivan, T. J. (2019). Plant richness and composition in hardwood forest understories vary along an acidic deposition and soil-chemical gradient in the northeastern United States. *Plant and Soil, 438*(1), 461-477. doi:10.1007/s11104-019-04031-y

Zech, M., Andreev, A., Zech, R., Müller, S., Hambach, U., Frechen, M., & Zech, W. (2010). Quaternary vegetation changes derived from a loess-like permafrost palaeosol sequence in northeast Siberia using alkane biomarker and pollen analyses. *Boreas, 39*(3), 540-550. doi:10.1111/j.1502-3885.2009.00132.x

Zhao, C., Yu, Z., Ito, E., & Zhao, Y. (2010). Holocene climate trend, variability, and shift documented by lacustrine stable-isotope record in the northeastern United States. *Quaternary Science Reviews, 29*(15), 1831-1843. doi:https://doi.org/10.1016/j.quascirev.2010.03.018

Zhao, Y., Yu, Z., & Zhao, C. (2010). Hemlock (Tsuga canadensis) declines at 9800 and 5300 cal. yr BP caused by Holocene climatic shifts in northeastern North America. *The Holocene, 20*(6), 877-886. doi:10.1177/0959683610365932

Figures

Figure 1: Topographic setting of the northeastern United States depicting the locations of the two study lakes. The blue polygon denotes the border of the Adirondack Park. The blue circle is the

location of the Global Network of Isotopes in Precipitation (GNIP) Ottawa station referenced in Section 5.4. ADK = Adirondack Mountains. OTT = Ottawa. ***<Figure should be displayed in color.>***

Figure 2: Schematic diagram of 48-hour air parcel back-trajectories to the ADK over a one year time period (2018) as computed by the NOAA Air Resources Laboratory public modelling software HYSPLIT, https://ready.arl.noaa.gov/HYSPLIT.php (Stein et al., 2015). Trajectories depicted in A through C are grouped according to source area. Figure 3D summarizes the relevant isotopic composition information pertaining to each trajectory grouping as discussed in Section 5.4. The oxygen isotope values are from Burnett et al. (2004), and the δD values are calculated from those values, and that study's reported local mean water line. ***<Figure should be displayed in color.>***

Figure 3: Large panels depict topography of the Heart Lake (A) and Moose Pond (B) catchment, showing catchment extent, lake area, coring locations (red circles) and stream inlets and outlets. Within the catchments the topography is shown as shaded relief. Outside the catchment elevation contours are shown in red. The contour interval is 5 m (Heart Lake) and 10 m (Moose Pond). Note the difference in scale between the two figures. Inset panels depict lake bathymetry with contour intervals of 5 m. ***<Figure should be displayed in color.>***

Figure 4: Bayesian age-depth models constructed for Moose Pond, Heart Lake (this study) and Heart Lake (Whitehead and Jackson, 1990) using Bacon v2.2. Increased shading indicates the greater likelihood the model will produce a result which passes through that section, and the solid red line depicts the weighted mean solution of the Monte Carlo simulations. Schematic diagrams of core stratigraphy are plotted above the depth axis. For detailed stratigraphic descriptions of Units A, B, and C, see Section 4.1. For model inputs and plots showing model stability, prior and posterior accumulation rate and memory as output by Bacon v2.2, see the Appendix, Figure A.1. ***<Figure should be displayed in color.>***

Figure 5: Stratigraphic, bulk chemical and compound-specific *n*-alkane concentration data for Heart Lake A and B cores plotted by age. Panels include stratigraphic sections (A), TOM (B), C:N ratios (C), bulk carbon-isotope ratios (D), *n*-alkane concentration values (E) and average chain length, ACL (F). Note the scale for ACL is at the top of the frame. All values occurring below 12.0 cal kyr BP (marked in italicized red on the y-axis) are age-unconstrained. Surface sediment data from Freimuth et al. (2020) are represented by points at ~0 cal kyr BP, and unconnected to the downcore values. ***<Figure should be displayed in color.>***

Figure 6: Same as in Figure 5 but showing results for Moose Pond. Age-unconstrained samples occur below 13.4 cal kyr BP (shown in italicized red on the y-axis). Note the difference in scale for TOM, $\delta^{13}C$ and *n*-alkane concentrations as compared to Figure 5. ***<Figure should be displayed in color.>***

Figure 7: Hydrogen-isotope ratios of *n*-C_{29} (orange squares) and *n*-C_{27} (red circles) for Moose Pond (A) and Heart Lake (B) plotted next to (C) reconstructed δD_{precip} values from Moose Pond (dark blue upright triangles) and Heart Lake (light blue reversed triangles). Panel (D) shows simplified stacked pollen assemblage zones from Whitehead and Jackson (1990). Black error bars on δD_{precip} values are the 1σ standard deviation on all pooled sample and standard replicates. Regional mean annual precipitation δD is shown with the small dashed blue line, and mean spring season (OIPC modeled precipitation data for the months of March to May) with the large dashed orange line. Pollen zone age boundaries are based on the updated age model produced for this study using Bacon v2.2. Pollen categories depicted are herbs, *Pinus* (pine), *Picea* (spruce), *Tsuga* (hemlock), *Betula* (birch), *Fagus* (beech) *Alnus* (alder) and other (22 other taxa). Herbs is composed of the following 11 categories: *Amaranthaceae*, *Ambrosia*-type, *Angiospermae* undiff. (herbs), *Artemisia*, *Asteraceae*, *Cyperaceae*, *Isoetes*, *Lycopodium-type*, *Poaceae*, *Polypodiophyta*,

and *Rumex*. Age-unconstrained samples in panels A, B and C from the base of Heart Lake and Moose Pond are outlined with thick black lines. The dashed black vertical line indicates age-unconstrained samples within the Heart Lake pollen zones in panel D. Average surface sediment hydrogen-isotope ratios recovered from the same coring site as this study and reported in Freimuth et al. (2020) are plotted at ~ 0 cal kyr BP. Note the difference in scale of the *n*-alkane δD values for Heart Lake and Moose Pond. ***<Figure should be displayed in color.>***

Figure 8: Modern water isotope data for the ADK modified from Freimuth et al. (2020). OIPC modeled seasonal precipitation for winter (December, January, February), spring (March, April May), summer (June, July, August) and fall (September, October, November) are represented by large circles labeled 1, 2, 3, and 4, respectively. Individual OIPC modeled monthly precipitation isotope values are plotted with labeled white circles. Surface water and xylem water samples collected at the study sites are represented by light blue circles and reversed triangles (Heart Lake) and dark blue squares and triangles (Moose Pond). Xylem water samples collected from one of 10 other ADK sites are shown with black crosses. Regional mean annual and mean spring season precipitation δD are represented by the dashed blue and orange lines, as described in Figure 7. RMWL = regional meteoric water line. REL = regional evaporation line. Equations for RMWL and REL were reported by Freimuth et al. (2020), and see that study for detailed descriptions of calculation method. Precip = precipitation. ***<Figure should be displayed in color.>***

Tables

Table 1: Lake and catchment information for Heart Lake and Moose Pond modified from Freimuth et al. (2020).

Site	Latitude	Longitude	Elevation (m)	Lake area (km^2)	Catchment area (km^2)	Catchment elevation range (m)	Stream Inlet #	Water depth at core site (m)	Maximum water depth (m)
Heart	44.18	-73.97	665	0.1	0.8	208	0	13.1	14
Moose	44.37	-74.06	475	0.7	17.4	710	≥1	20	22

Table 2: Radiocarbon sample information and results from NOSAMS Laboratory.

Sample ID*	Lake	Depth below sediment-water interface (cm)	Accession #	^{14}C Age BP	^{14}C Age BP Error
HRT-B-144.5-145.5	Heart	145	OS-134712	675	± 20
HL2-188	Heart	188	OS-138212	1,730	± 20
HL3-298	Heart	298	OS-137959	2,950	± 20
HL4-358	Heart	358	OS-138210	3,910	± 30
HL4-418	Heart	418	OS-137960	4,790	± 25
HRT17-2A-1L-5	Heart	505	OS-146236	5,580	± 25
HL6-598	Heart	598	OS-138207	8,130	± 45
HRT17-2A-1L-7	Heart	689	OS-146262	9,380	± 35
HRT17-2A-1L-7	Heart	720-721	OS-146263	10,950	± 45
ML-B-121-121.5	Moose	121.25	OS-134714	1,500	± 20
MSE17-1A-1L-2	Moose	250	OS-146259	2,710	± 20
ML3-370.5	Moose	370.5	OS-138213	4,420	± 25
ML4-431	Moose	431	OS-138209	5,770	± 30
ML5-530.5	Moose	530.5	OS-138214	8,030	± 40
ML6-684	Moose	684	OS-138211	11,200	± 70
MSE17-1A-1L-6	Moose	626-627	OS-146260	10,400	± 45
MSE17-1A-1L-7	Moose	693-695	OS-146261	11,550	± 50

* All samples dated where non-aquatic, firm, woody plant or leaf material.

Figure 1

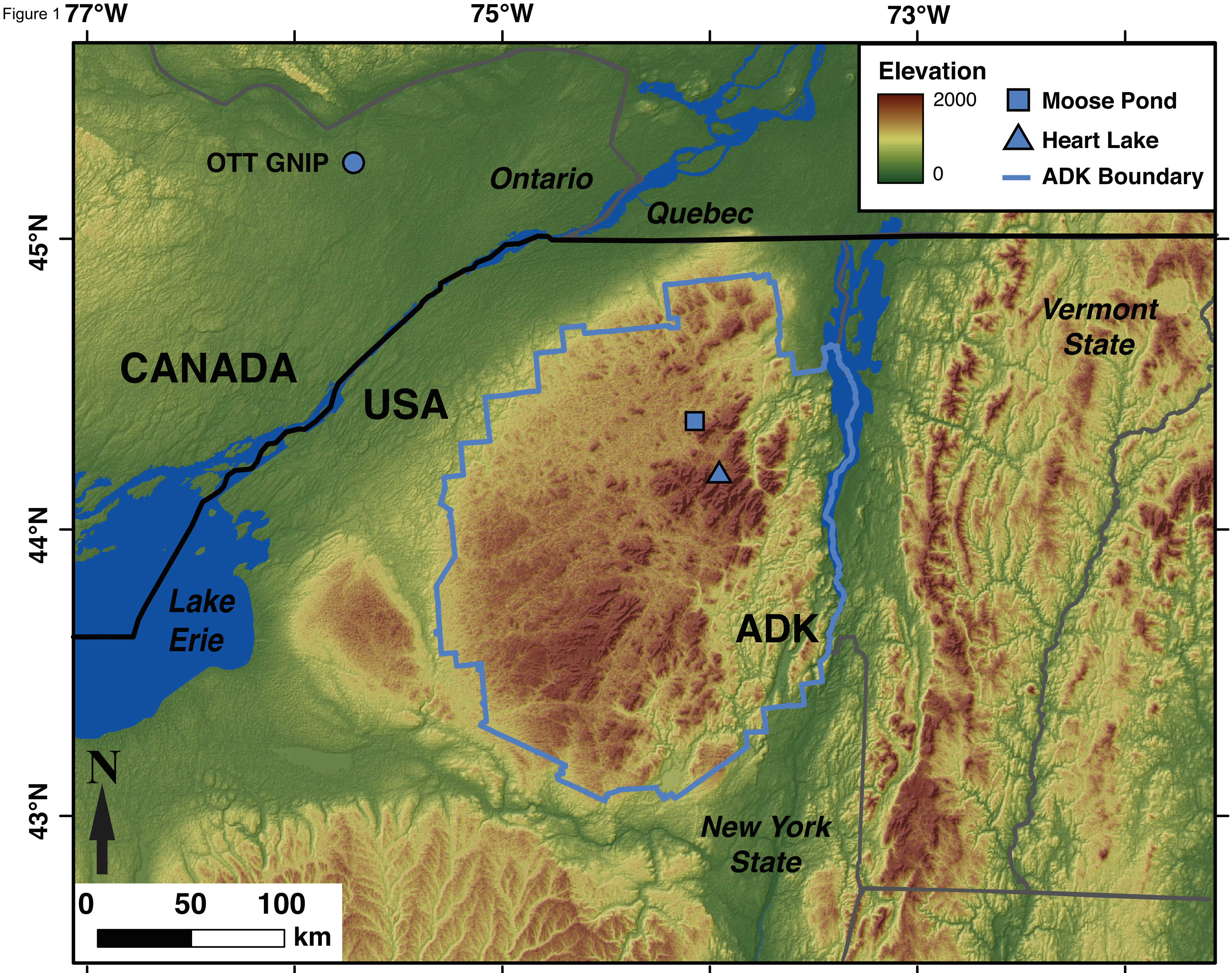

77°W
75°W
73°W
45°N
44°N
43°N
Elevation
2000
0
Moose Pond
Heart Lake
ADK Boundary
OTT GNIP
Ontario
Quebec
CANADA
USA
Vermont State
Lake Erie
ADK
New York State
N
0
50
100
km

Figure 2

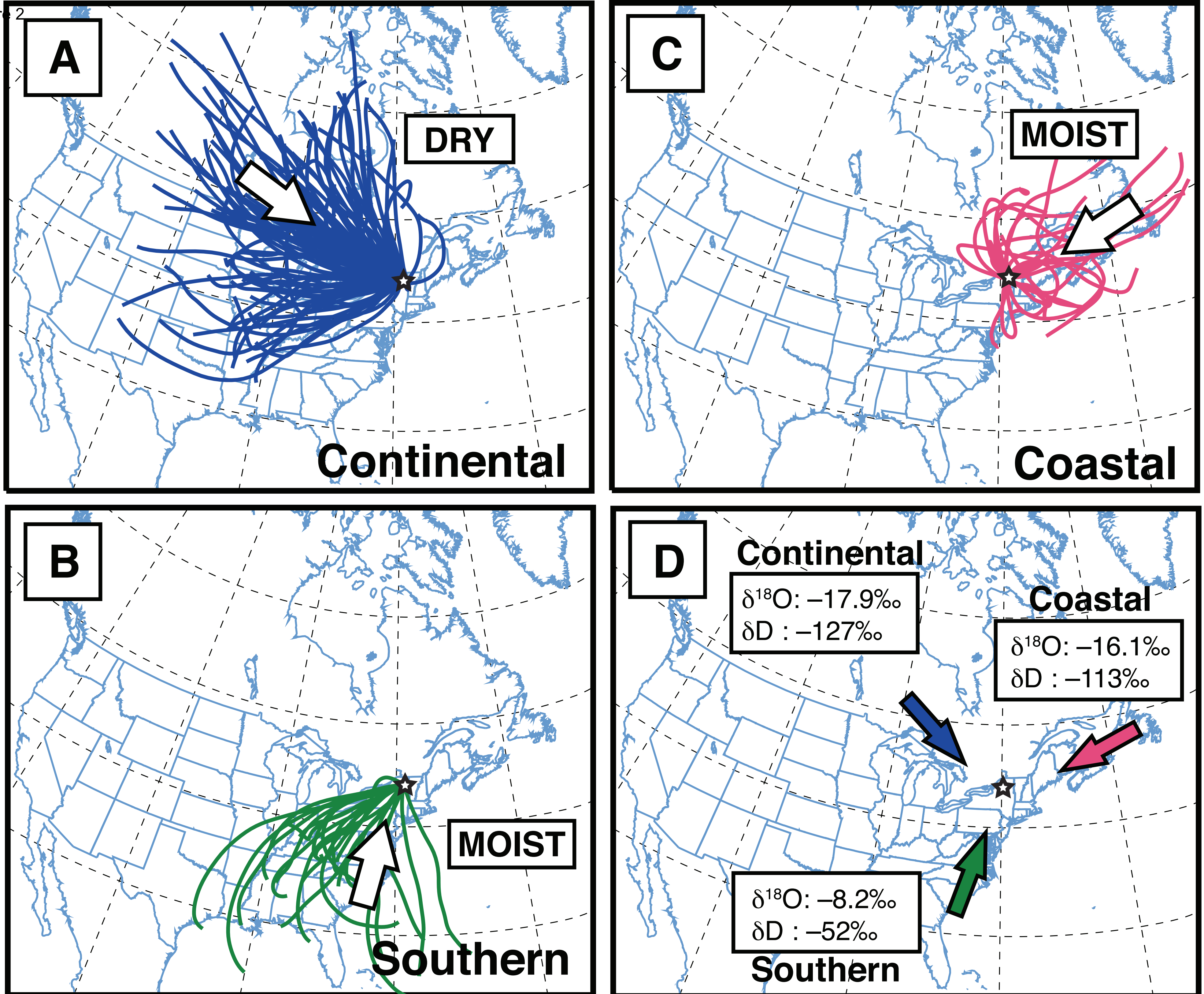

A
DRY
Continental
C
MOIST
Coastal
B
MOIST
Southern
D
Continental
δ18O: –17.9‰
δD : –127‰
Coastal
δ18O: –16.1‰
δD : –113‰
δ18O: –8.2‰
δD : –52‰
Southern

Figure 3A

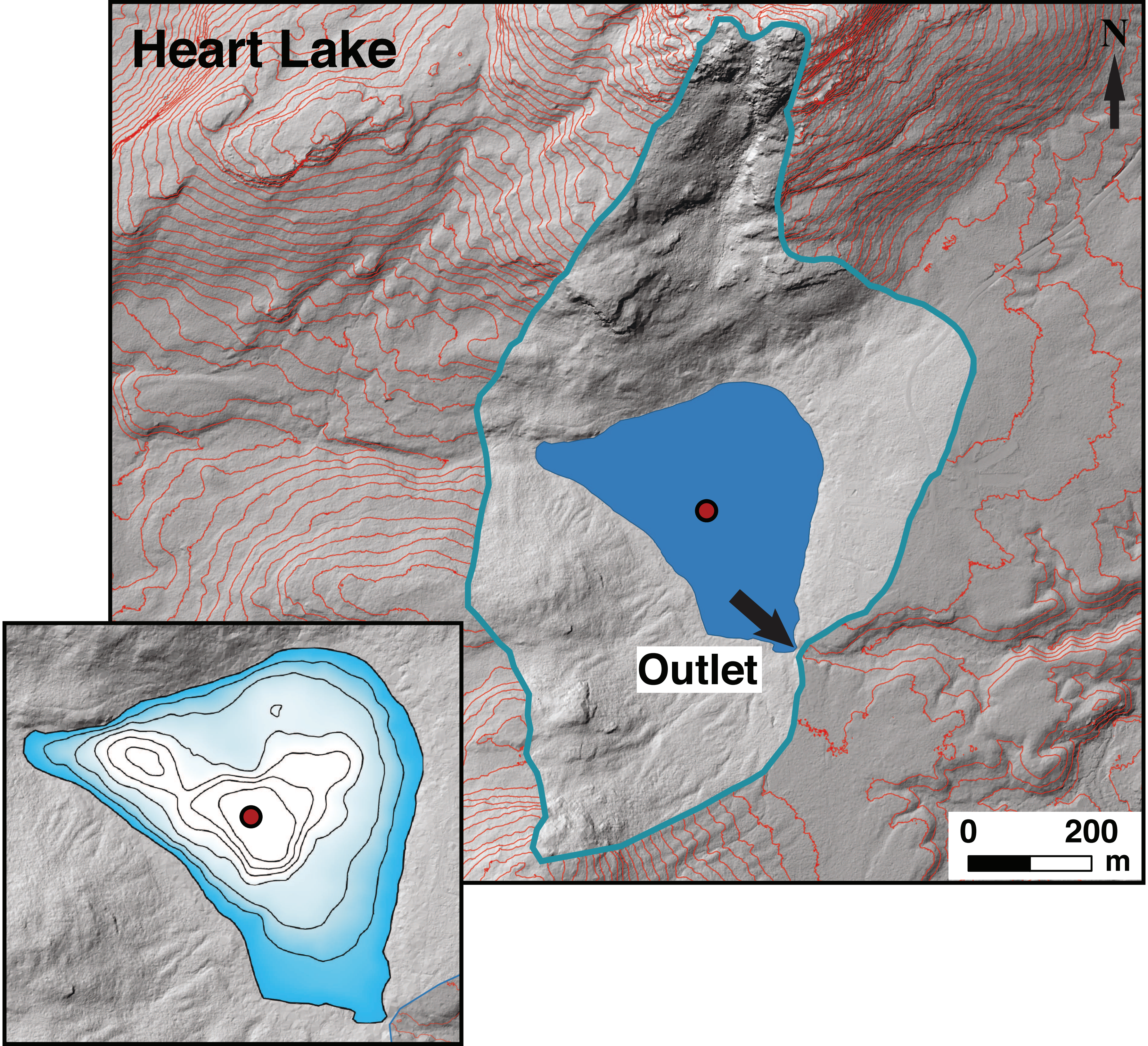

Figure 3B

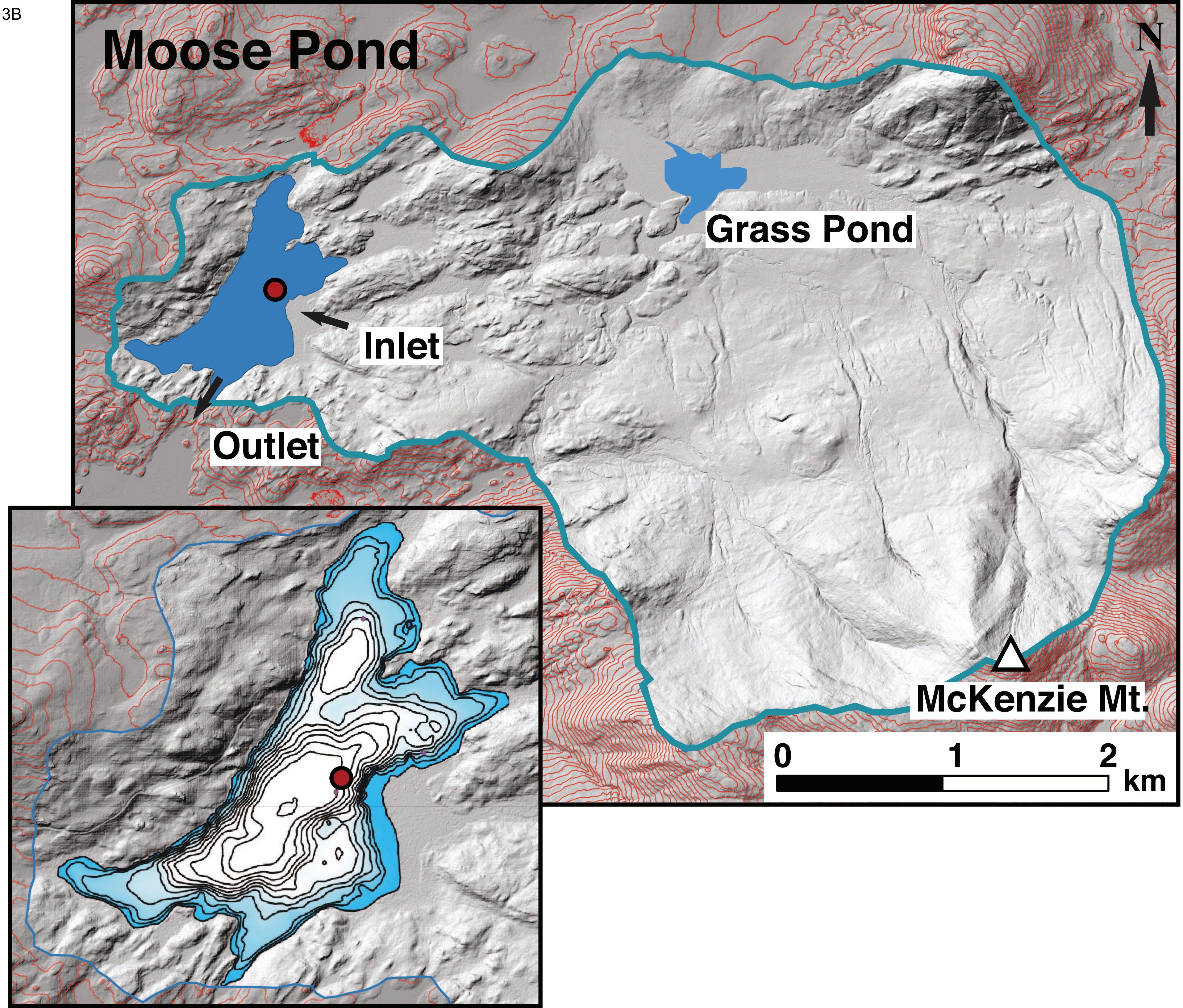

Figure 4

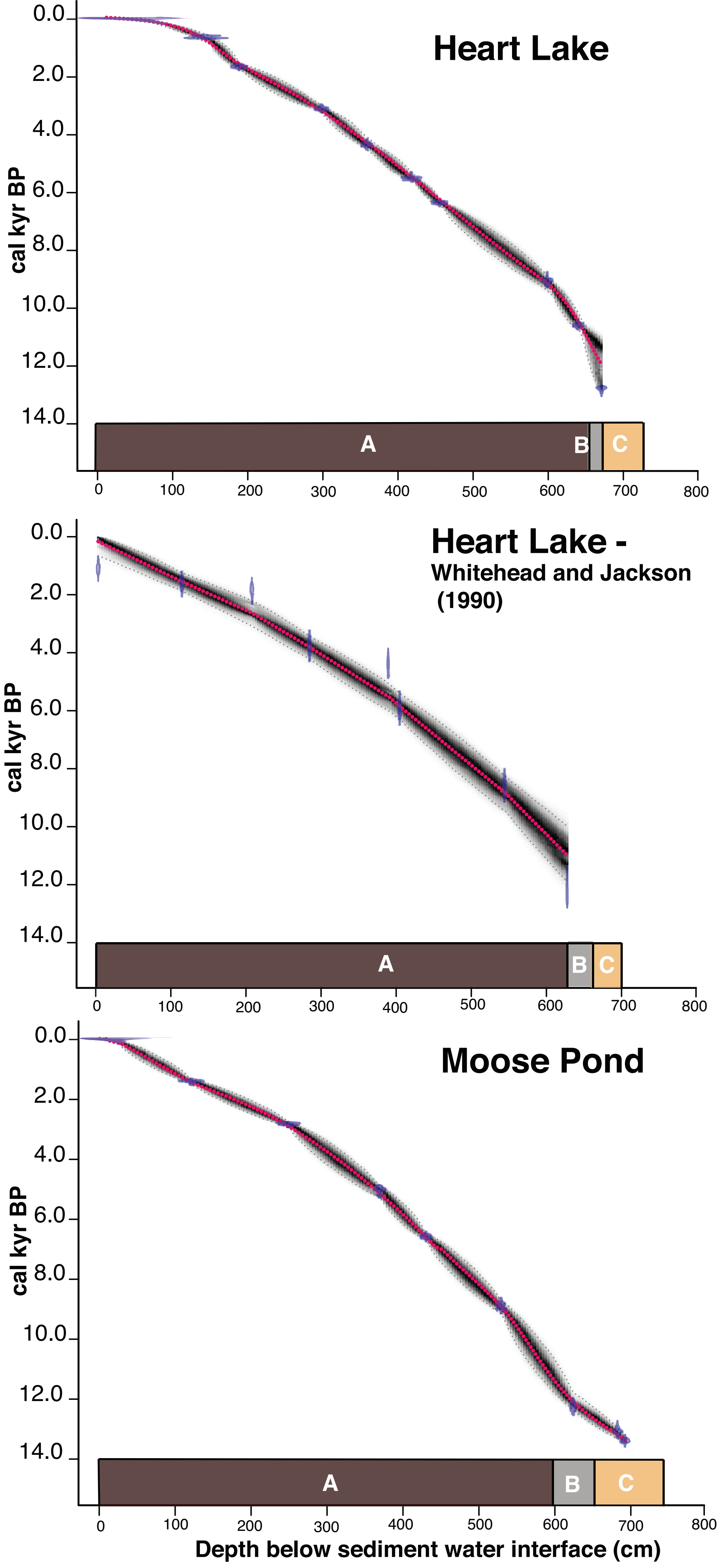

Heart Lake
Heart Lake -
Whitehead and Jackson
(1990)
Moose Pond
cal kyr BP
0.0
2.0
4.0
6.0
8.0
10.0
12.0
14.0
A
B
C
0
100
200
300
400
500
600
700
800
Depth below sediment water interface (cm)

Figure 5

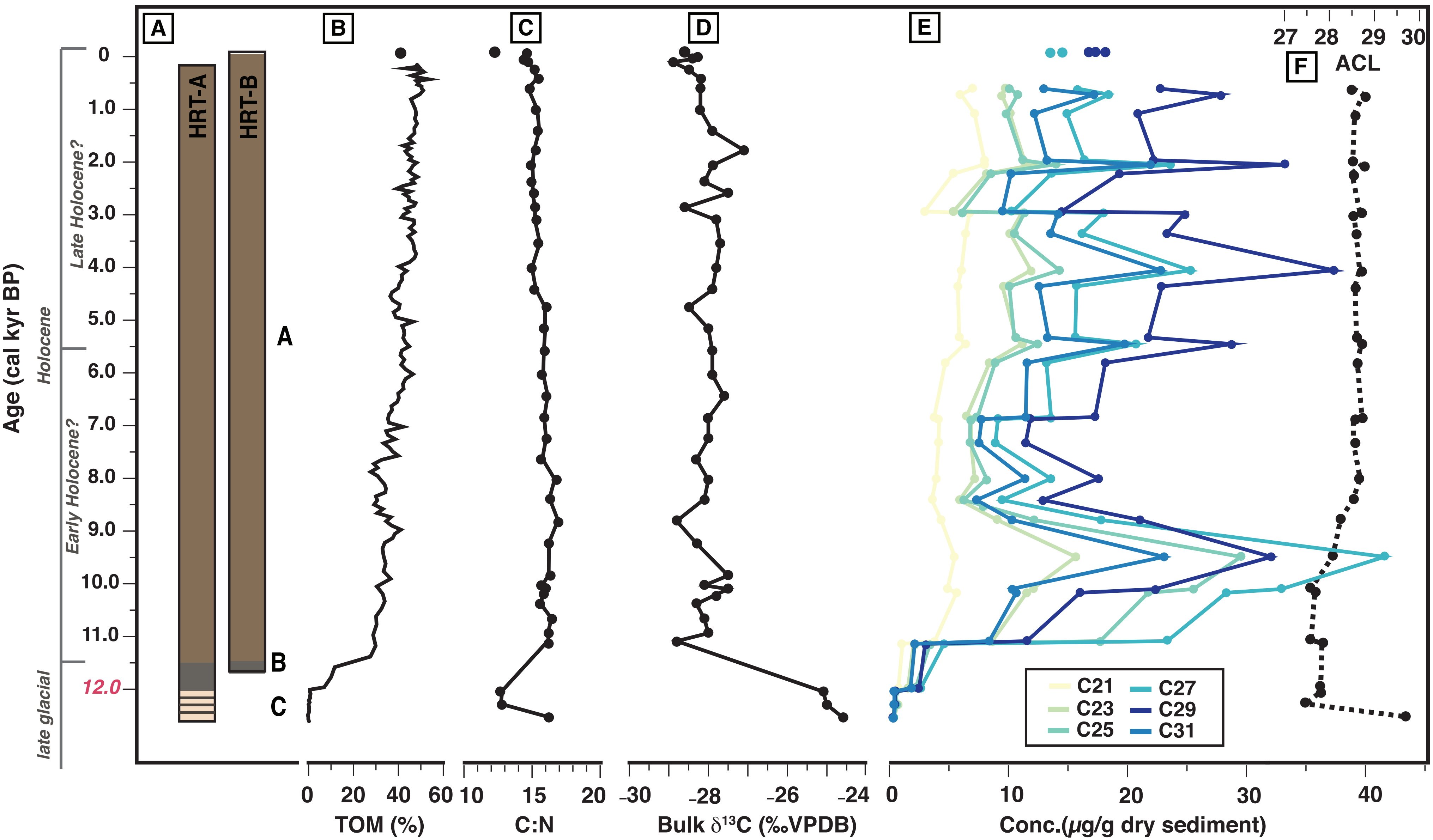

A
B
C
D
E
F
ACL
27
28
29
30
HRT-A
HRT-B
A
B
C
Age (cal kyr BP)
Holocene
Late Holocene?
Early Holocene?
late glacial
0
1.0
2.0
3.0
4.0
5.0
6.0
7.0
8.0
9.0
10.0
11.0
12.0
0
20
40
60
TOM (%)
10
15
20
C:N
-30
-28
-26
-24
Bulk δ13C (‰VPDB)
0
10
20
30
40
Conc.(μg/g dry sediment)
C21
C23
C25
C27
C29
C31

Figure 6

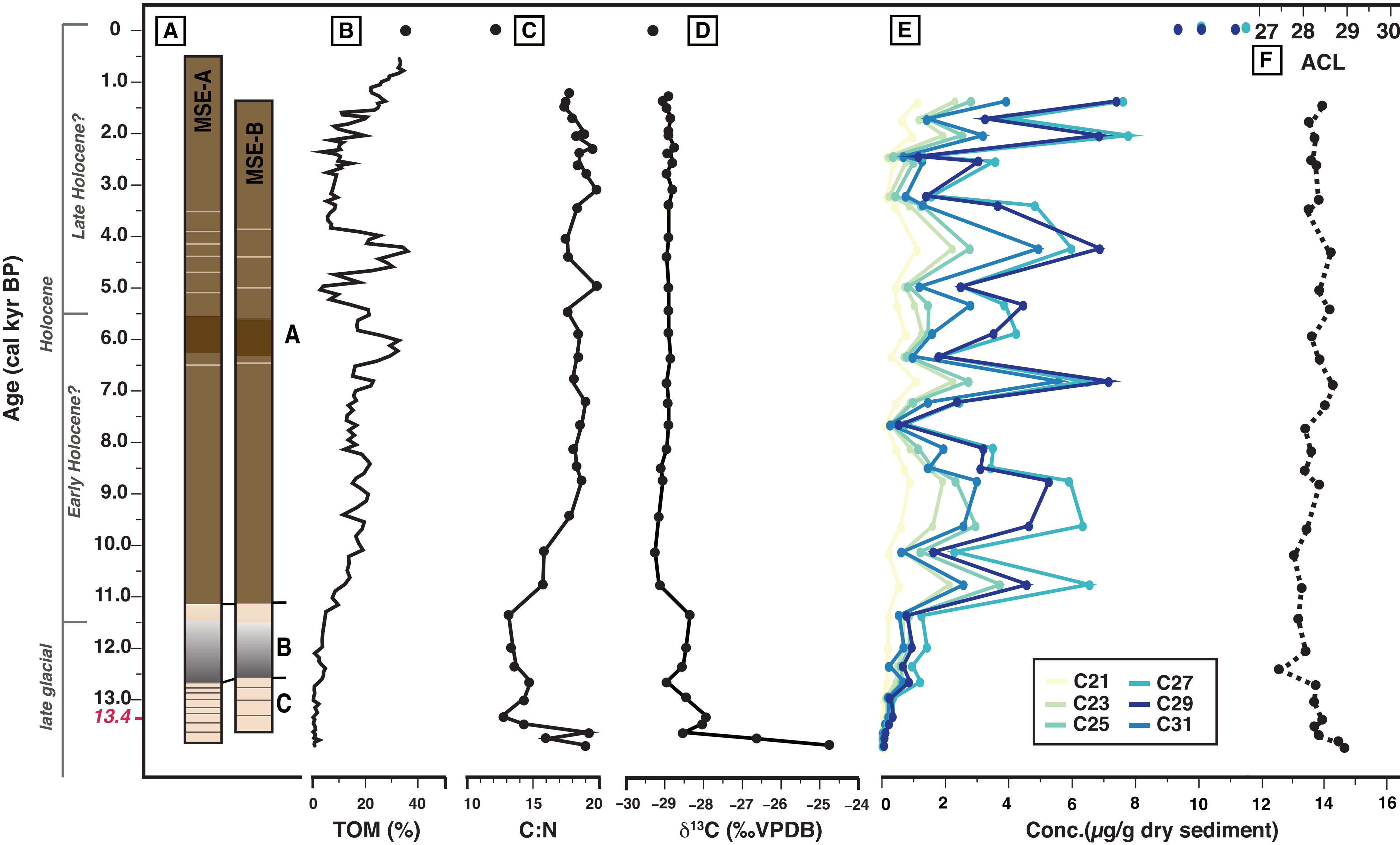

Age (cal kyr BP)
Holocene
late glacial
Late Holocene?
Early Holocene?
0
1.0
2.0
3.0
4.0
5.0
6.0
7.0
8.0
9.0
10.0
11.0
12.0
13.0
13.4
A
B
C
D
E
F
ACL
MSE-A
MSE-B
27
28
29
30
TOM (%)
C:N
δ13C (‰VPDB)
Conc.(µg/g dry sediment)
C21
C23
C25
C27
C29
C31

Figure 7

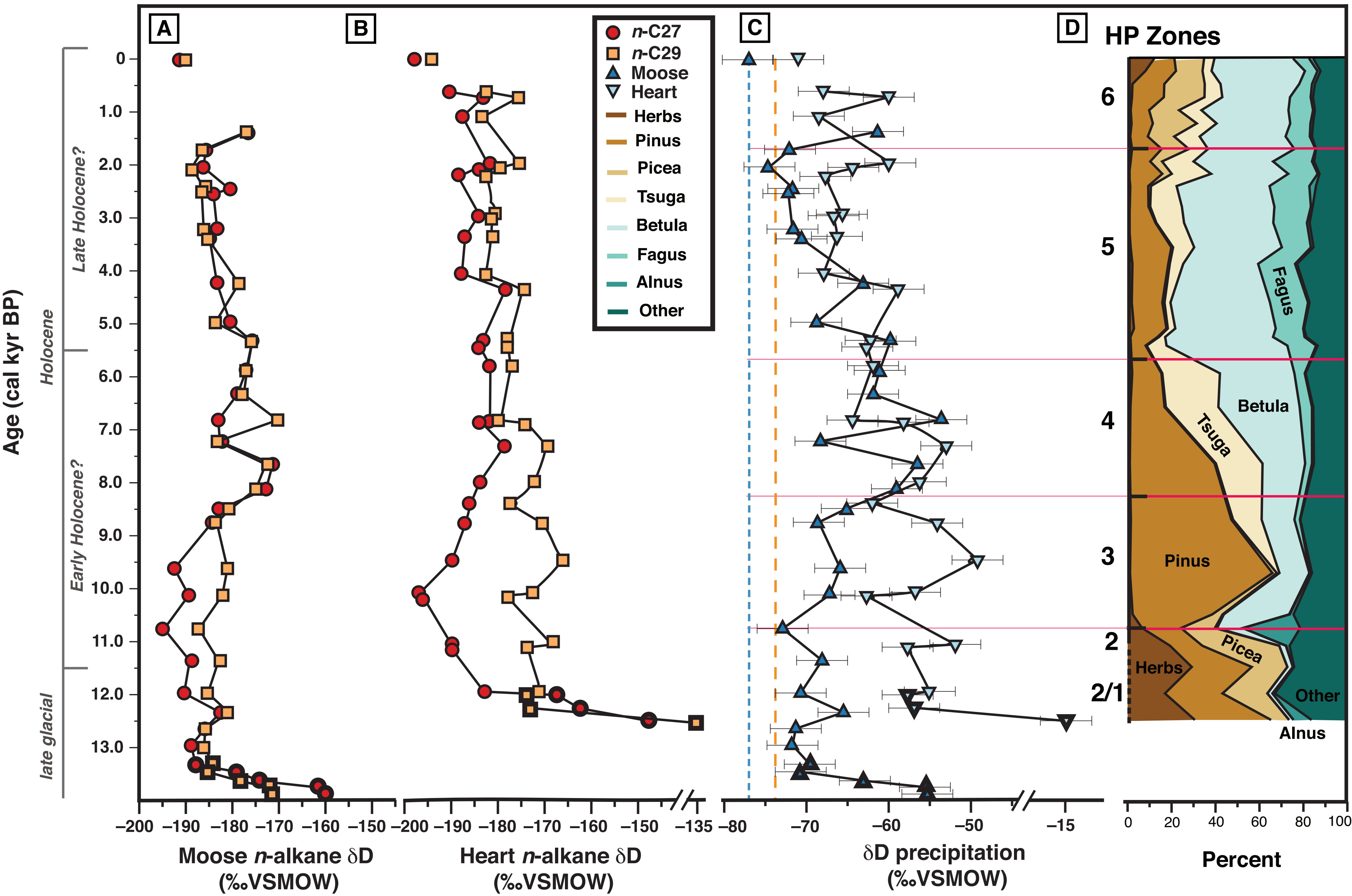
A
B
C
D
HP Zones
n-C27
n-C29
Moose
Heart
Herbs
Pinus
Picea
Tsuga
Betula
Fagus
Alnus
Other
Age (cal kyr BP)
Holocene
Late Holocene?
Early Holocene?
late glacial
0
1.0
2.0
3.0
4.0
5.0
6.0
7.0
8.0
9.0
10.0
11.0
12.0
13.0
6
5
4
3
2
2/1
Fagus
Betula
Tsuga
Pinus
Picea
Herbs
Other
Alnus
−200 −190 −180 −170 −160 −150
Moose n-alkane δD (‰VSMOW)
−200 −190 −180 −170 −160 −150 −135
Heart n-alkane δD (‰VSMOW)
−80 −70 −60 −50 −15
δD precipitation (‰VSMOW)
0 20 40 60 80 100
Percent

Figure 8

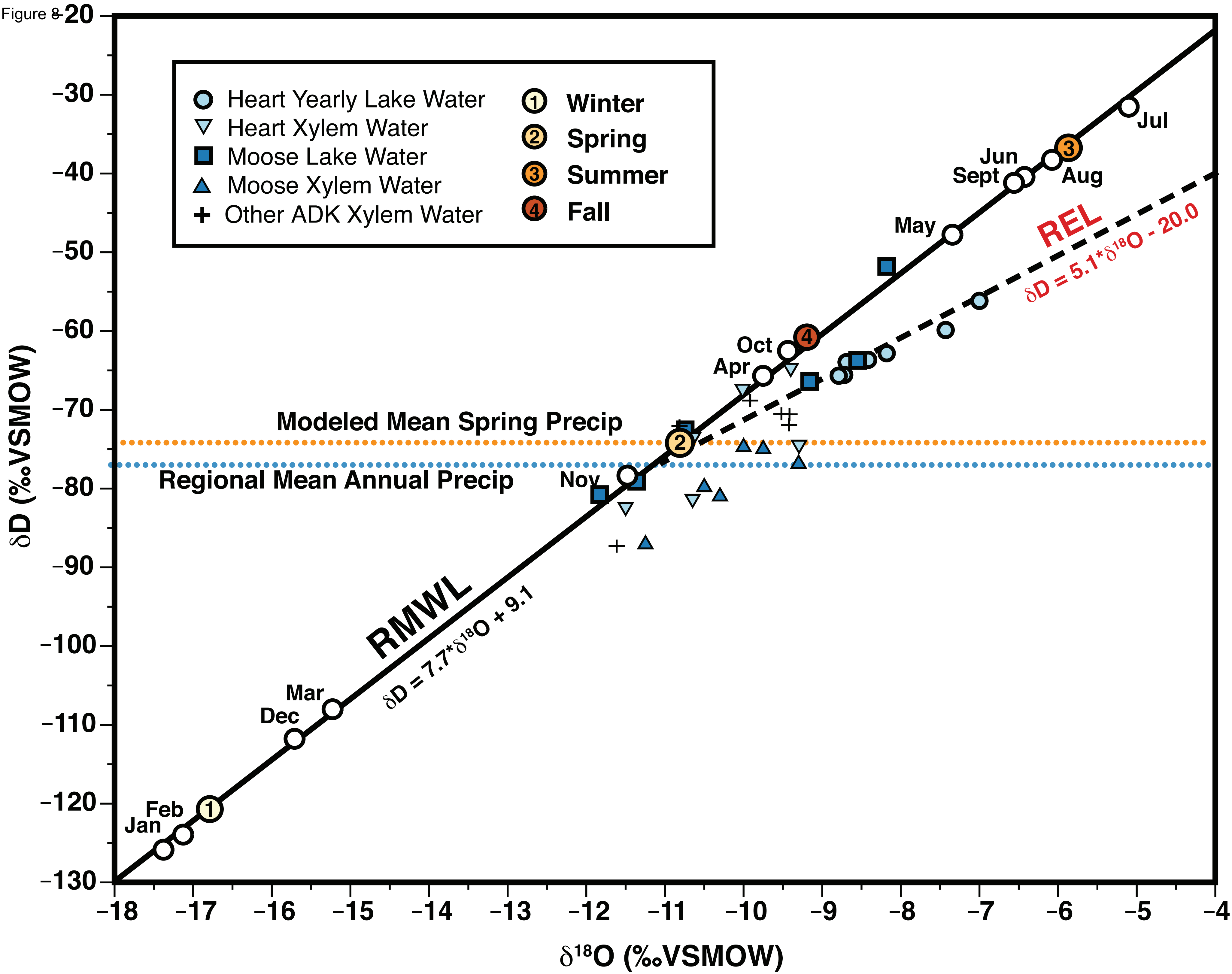

Heart Yearly Lake Water
Heart Xylem Water
Moose Lake Water
Moose Xylem Water
Other ADK Xylem Water
Winter
Spring
Summer
Fall
Jul
Jun
Sept
Aug
May
REL
δD = 5.1*δ18O - 20.0
Oct
Apr
Modeled Mean Spring Precip
Regional Mean Annual Precip
Nov
RMWL
δD = 7.7*δ18O + 9.1
Mar
Dec
Feb
Jan
δD (‰VSMOW)
δ18O (‰VSMOW)